AD-A122 539 STUDY OF THE DEPENDENCE OF MICROSEGREGATION ON CRITICAL 1/1
SOLIDIFICATION PA..(U) UNITED TECHNOLOGIES RESEARCH
CENTER EAST HARTFORD CT E M BREINAN ET AL. OCT 82
UNCLASSIFIED UTRC/R82-915797-2 N00014-79-C-0649 F/G 20/11 NL

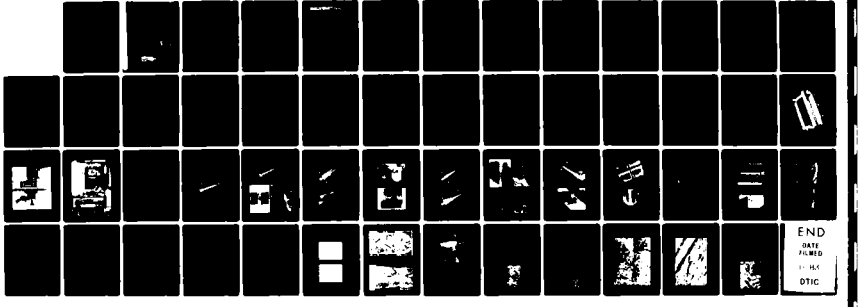

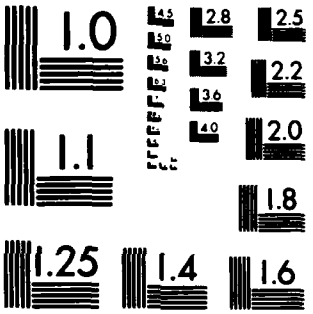

MICROCOPY RESOLUTION TEST CHART
NATIONAL BUREAU OF STANDARDS-1963-A

R82-915797-2

(12)

STUDY OF THE DEPENDENCE OF MICROSEGREGATION ON CRITICAL SOLIDIFICATION PARAMETERS IN RAPIDLY- QUENCHED STRUCTURES

Prepared by

E.M. Breinan
D.B. Snow

ANNUAL TECHNICAL REPORT

Contract N00014-79-C-0649
Project No. NR 031-825/5-28-81 (471)

for

Office of Naval Research
Department of the Navy
Arlington, Virginia 22217

by

UNITED TECHNOLOGIES RESEARCH CENTER
East Hartford, Connecticut 06108

UNCLASSIFIED

SECURITY CLASSIFICATION OF THIS PAGE (When Data Entered)

REPORT DOCUMENTATION PAGE	READ INSTRUCTIONS BEFORE COMPLETING FORM
1. REPORT NUMBER: R82-915797-2	2. GOVT ACCESSION NO.: A122 539
3. RECIPIENT'S CATALOG NUMBER:	
4. TITLE (and Subtitle): STUDY OF THE DEPENDENCE OF MICROSEGREGATION ON CRITICAL SOLIDIFICATION PARAMETERS IN RAPIDLY-QUENCHED STRUCTURES	5. TYPE OF REPORT & PERIOD COVERED: Annual Technical Report Oct. 1981 - Sept. 1982
	6. PERFORMING ORG. REPORT NUMBER:
7. AUTHOR(s): E. M. Breinan and D. B. Snow	8. CONTRACT OR GRANT NUMBER(s): N00014-79-C-0649
9. PERFORMING ORGANIZATION NAME AND ADDRESS: United Technologies Research Center East Hartford, CT 06108	10. PROGRAM ELEMENT, PROJECT, TASK AREA & WORK UNIT NUMBERS:
11. CONTROLLING OFFICE NAME AND ADDRESS: Office of Naval Research Department of the Navy Arlington, VA 22217	12. REPORT DATE: October 1982
	13. NUMBER OF PAGES:
14. MONITORING AGENCY NAME & ADDRESS (if different from Controlling Office):	15. SECURITY CLASS. (of this report): Unclassified
	15a. DECLASSIFICATION/DOWNGRADING SCHEDULE:

16. DISTRIBUTION STATEMENT (of this Report)

DISTRIBUTION STATEMENT A
Approved for public release
Distribution Unlimited

17. DISTRIBUTION STATEMENT (of the abstract entered in Block 20, if different from Report)

18. SUPPLEMENTARY NOTES

19. KEY WORDS (Continue on reverse side if necessary and identify by block number)

Laser Welding
Narrow Gap Laser Welding
Laser Materials Processing
Titanium Martensite
Microsegregation
Rapidly Quenched Microstructure
Ti-6Al-4V
As-Welded Mechanical Properties
LAYERGLAZE Processing

20. ABSTRACT (Continue on reverse side if necessary and identify by block number)

Laser welds of 1.27 and 2.54 cm thick Ti-6Al-4V (wt%) plate separated by a 4 mm straight-sided gap were achieved with the aid of the addition of solution blend Ti-6Al-4V powder to the weld gap (the powder-feed LAYERGLAZE process). A continuous CO_2 laser was utilized in the unstable resonator mode with a set beam power of 5 kW, focused by a copper mirror of 45.7 cm focal length. Each successive layer of feedstock filled the gap width, and

DD FORM 1 JAN 73 1473 EDITION OF 1 NOV 65 IS OBSOLETE
S/N 0102-LF-014-6601

UNCLASSIFIED
SECURITY CLASSIFICATION OF THIS PAGE (When Data Entered)

#20. cont'd

was overlaid by another until the gap was filled. Ambient temperature tests of cross-weld tensile and impact specimens revealed no fusion zone strength reduction but a somewhat decreased toughness with respect to the annealed base metal. The average fusion zone microhardness was 417 VHN vs 342 outside the HAZ, due primarily to an increase in oxygen content in the fusion zone. The fusion zone grain structure was distinctively columnar, with grains traversing many successive deposited layers. No grain boundary α phase was detected; the grains consisted entirely of fine α' HCP martensite, internally twinned and faulted, with a wide range of lath lengths and a high dislocation density. No grain boundary or interdendritic segregation was detected by TEM/STEM EDS analysis.

UNITED TECHNOLOGIES RESEARCH CENTER

UNITED TECHNOLOGIES

East Hartford, Connecticut 06108

R82-915797-2

Study of the Dependence of Microsegregation on Critical Solidification Parameters in Rapidly-Quenched Structures

ANNUAL TECHNICAL REPORT
Contract N00014-79-C-0649

REPORTED BY Edward M. Breinan
E. M. Breinan

David B. Snow
D. B. Snow

APPROVED BY Anthony J. Giamei
A. F. Giamei, Principal Scientist
Alloy & Process Research

DATE OCT. 1982

NO. OF PAGES _____ **COPY NO.** _____

R82-915797-2

Study of the Dependence of Microsegregation on Critical Solidification Parameters in Rapidly-Quenched Structures

TABLE OF CONTENTS

R82-915797-2

Study of the Dependence of Microsegregation on Critical Solidification Parameters in Rapidly-Quenched Structures

INTRODUCTION

During the past few years, the perpetual need for better performance in advanced military aircraft and warships has led to the development of structural and engine materials with improved mechanical property combinations. In the case of nickel, titanium and aluminum base alloys, such improvements have become increasingly difficult to achieve through new alloy development alone. This situation has led to a greater awareness that significant advances in materials properties can be made through the development of advanced, precisely controlled processing techniques, which beneficially change the alloy microstructure during either consolidation or joining. One such technology is laser materials processing, which has been developed at the United Technologies Research Center as a result of its traditional interest in improved materials and continuous, high power carbon dioxide laser systems. A specific example is the LAYERGLAZE^{SM} Process (Refs. 1-3), in which wire or powder feedstock is introduced into the moving laser beam-metal interaction zone. By this technique it is possible to achieve the bulk consolidation of rapidly solidified alloys (10^4-10^5°C/s) in the form of sequentially overlapping layers. The correct choice of beam intensity and energy distribution on the workpiece will reduce the amount of retained porosity to very low levels (Refs. 1,4), thus eliminating the need for subsequent densification. A controlled amount of substrate melting occurs during the deposition of each layer, and this ensures complete interlayer mixing and consequent mechanical integrity between layers.

An important requirement for successful LAYERGLAZE processing is the capacity of an alloy to accommodate the high stresses and consequent high strain rates imposed by the rapid solid state cooling of each layer. Research at UTRC has demonstrated that titanium base alloys are particularly compatible with the LAYERGLAZE Process in this respect (Ref. 4). In addition, laser welded and LAYERGLAZE processed titanium alloys have been reported to contain very low levels of entrapped porosity in most cases (Refs. 4-6), with one exception (Ref. 7). Further, the mechanical properties of as-laser welded, near-α and α-β titanium alloys are comparable to, and in some cases more ductile than, welds made by gas/tungsten arc (GTA) or electron beam welding (Refs. 6,8). These

favorable structure/property characteristics of laser processed titanium are augmented by two factors which make LAYERGLAZE processing particularly applicable to the narrow gap welding of thick plates: (A) the deep penetration characteristics of high-power lasers achieved by the creation of a steady-state vapor column (the "keyhole" effect) and by sidewall reflection within the gap (Ref. 9), and (B) the greater effectiveness of feedstock introduction into the gap in powder rather than wire form. It was the main objective of the first phase of the research program described herein to demonstrate that narrow-gap welding of Ti-6Al-4V plate could be achieved by this means without machining the weld gap into a "v" configuration or sacrificing the superior mechanical properties of autogeneous laser welds in this alloy. The data reported herein show that this objective was successfully achieved. Further, they suggested that it will be feasible to attempt to achieve additional ductility and strength enhancement of laser-processed titanium alloys through deliberate changes in the powder feedstock composition and the inherently rapid solidification of the fusion zone.

EXPERIMENTAL PROCEDURE

The titanium alloy utilized for this research program was Ti-6Al-4V (wt%), purchased in the mill-annealed condition in thicknesses of 1.27 and 2.54 cm. The specimen sides were machined so that two pieces could be joined to form the narrow gap configurations shown in Fig. 1. The specimen configuration for the first series of welds was formed by placing two matching pieces with 2 mm lands (Fig. 1) in a positioning fixture (Fig. 2) so as to form a 4 mm wide, straight-sided narrow gap. This fixture was equipped with retention bars to prevent warpage of the welded specimens due to solidification shrinkage as the gap was filled.

The protective atmosphere chamber and the work station utilized for all LAYERGLAZE/narrow-gap welds are shown in Figs. 3 and 4. The laser was initially focused to a 3.18 mm diameter spot at the bottom of the gap by means of a 47 cm focal length copper mirror positioned so that the bottom of the gap lay 2.86 cm below its focal plane. Thus the beam diameter was less than the gap width at all vertical heights within the gap.

The first series of welds were made with 1.27 cm thick specimens at a welding speed of 2.12 cm/s. The laser power was set at 5 kW, so that a power of ~3.76 kW was delivered to the workpiece at an intensity of ~47.5 kW/cm^2. The specimen height was lowered every four passes to compensate for material accumulation at the bottom of the gap and thus maintain a relatively constant laser power input to the weld.

Transport of the powder feedstock into the weld gap was accomplished by gravity feed assisted by mechanical vibration as described in Ref. 1. An attempt was made to utilize both mechanically blended elemental powder and prealloyed powder. However, an erratic and noncolumnar flow pattern was experienced with the elemental powder, so that prealloyed powder was used for all but the first 1.27 cm specimen. The specifications of both types powder feedstock are described in Tables I and II.

Specimen contamination was minimized by chemically cleaning the Ti-6Al-4V plate a few minutes prior to welding in a solution of 30% nitric and 3% hydrofluoric acid in water, followed by a water rinse and drying with forced air. The protective chamber was filled with helium during welding, continuously introduced at a flow rate of 5.7 m^3/h.

The welding parameters utilized for the first and second series of specimens are described in Tables III and IV, respectively. Specimen No. 7 (Table IV) was welded with the use of a 51-cm focal length oscillating mirror, which was driven by compressed air so as to rotate the focal spot in a circle at 2000 rpm. As

noted in Table IV, this innovation was unsuccessful and was replaced by a 47 cm fixed focusing mirror for the remainder of the specimens. A shaker table was used underneath specimens 7 and 8 during welding, but was removed in the case of specimens 9 and 10 as it appeared to promote sidewall bridging of the fusion zone above the bottom of the weld, thus causing macroscopic voids. Specimens 9 and 10 were welded with preplaced powder feedstock in an attempt to completely eliminate this problem, a procedure which also allowed the entire height of the gap to be filled in twelve passes. The specimen height was lowered by 3.8 mm after the first four passes, but was not lowered again as the beam was about to touch the sidewalls of the gap.

The macroscopic structure of the welds were examined in transverse section. Specimen No. 9 was evaluated more extensively, including transverse microhardness variation across the fusion zone at three different heights, and detailed microstructural observation by light microscopy and analytical electron microscopy using a Philips EM400T TEM/STEM.

Mechanical test specimens were prepared from sections cut transverse to the welding direction. A typical arrangement of test specimens within such a section is shown by Fig. 5. Both standard and one-half size Charpy bars were prepared with root, side and edge notch orientations. Impact tests were conducted at room temperature on an instrumented apparatus according to standard ASTM procedures. Tensile specimens with 2.61 gage length and 3.18 mm gage diameter were tested at room temperature at a strain rate of 0.01 min^{-1} (1.7×10^{-4} s^{-1}).

RESULTS

A. Structure of Weld Specimens 3-8

The macrostructure and transverse microstructure of weld specimens 3-8 are shown in Figs. 6-12. Figure 6 shows the relatively rough surface of the fusion zone of weld specimen 3. This weld had reasonably good integrity, but several subsequently-welded specimens were superior in this respect and thus it was not examined in detail. A macroscopic view of weld specimen no. 4, together with its cross-sectional microstructure, is shown in Fig. 7. The lower-magnification view of the cross section clearly shows the distinctive columnar grain structure generated by the LAYERGLAZE Process (Refs. 1,2,4), formed by the sequential epitaxial nucleation of each grain as each layer is deposited. The orientation of the columnar grains tends to become more vertically oriented as the center line of the fusion zone is approached. This is in contrast to the columnar microstructure of autogeneous, deep-penetration laser welds in α-β titanium alloys reported in the literature (Refs. 6-8), in which the grains are oriented in a direction more uniformly perpendicular to the plane of the weld center line. This difference in the Layerglazed microstructure reflects an additional heat flux toward the bottom of each layer during its solification, in addition to that toward the sides of the fusion zone. Figure 7 also shows an example of sidewall fusion between two layers. Eventually it was possible to substantially eliminate this type of defect, although it occurred to varying degrees in weld specimens 1-8.

Specimen no. 5 was the first attempt to weld to a depth of 2.54 cm. The set power of 5 kW (~3.9 kW at the weld) and 127 cm/s traverse speed (Table III) did not provide quite enough energy for the fusion zone to reach all the way through the bottom step in the weld gap (Fig. 8). In a later weld this problem was corrected by reducing the traverse speed by a factor of 2. The effect of insufficient fusion at the bottom and mid-height of one cross-sectional area of weld no. 5 is further illustrated in Fig. 9, although interlayer porosity was absent throughout most of the weld.

By way of contrast, the 2.54 cm-thick specimen welded from both sides, with the step bridging the gap placed at the "central" (mid-thickness) position (Fig. 1), displayed a fusion zone with generally better integrity since both exposed surfaces were now the top crown of the weld (Fig. 10). The uniformity of the microstructure in cross section is shown in Fig. 11, although the fusion zone was still not completely filled in at the bottom corner of one side. The variation in grain structure from vertically columnar at the center line to smaller and nearly horizontal at the edge of the heat-affected zone, typical of all welds made in this study, is also illustrated.

Both an oscillating focusing mirror and a shaker table attached under the Ti-6-4 plate were utilized for weld no. 7 (second series, Table IV) in an attempt to promote complete melting of the powder feedstock at the bottom of the weld gap by rapidly moving the point of beam impingement within the gap. However, this combination caused extensive sidewall fusion with the result that the weld gap became completely bridged well above the bottom of the cavity. The oscillating mirror was replaced by the focusing mirror utilized for all previous specimens (Table IV), although the use of the shaker table was retained for weld no. 8. No problems were apparent during the welding of this specimen, and its macroscopic appearance was quite satisfactory (Fig. 12). However, examination of several weld cross-sections revealed that sidewall bridging had occurred along its entire length. Apparently enough sidewall fusion had occurred to trap and melt the powder above the bottom of the gap with sufficient efficiency to completely close it over, thus causing a macroscopic cavity (Fig. 12).

In order to ensure that subsequent specimens would have sufficient integrity for mechanical property evaluation, the shaker table was eliminated, and the powder feedstock was preplaced at the bottom of the weld gap prior to each laser pass. In weld specimen no. 9, each layer of powder was added to a depth of ~2.5 mm, which allowed the 2.5 cm weld gap to be filled with twelve laser passes. As shown by Fig. 13, weld specimen no. 9 had a good surface appearance, with no evidence of macroscopic porosity when sectioned. However, some instance of $\leq$0.2 mm interlayer porosity were observed.

Weld no. 10 differed from no. 9 in that it was a double sided weld with two weld gaps of 1.27 cm depth. Welding was conducted under the same conditions that were employed for specimen no. 9. However, when an attempt was made to weld the second side of specimen no. 10, the degree of warpage after the second laser pass closed the gap sufficiently to cause sidewall bridging and consequent macroscopic cavity formation as illustrated by Fig. 15. However, the fusion zone of the first side appeared to have the high quality of weld no. 9, in which only small spherical voids ($\leq$50μm) were infrequently observed at the interface between some of the layers (Fig. 16).

B. Chemical Analysis and Microhardness

Samples of the fusion zone and of the surrounding unwelded plate were taken from weld specimen no. 9 for chemical analysis. The results (Table V) show that there was some increase in the average oxygen content of the fusion zone. Some degree of oxygen increase in the fusion zone was anticipated because of the 0.17 wt% O content of the powder feedstock and its sequential deposition in layers. To examine this phenomenon in more detail, it was assumed that oxygen in solid solution would produce a measurable hardness increase. Consequently, horizontal microhardness profiles of one transverse cross section of weld specimen

no. 9 were obtained near the top surface at mid height and near the bottom surface across the welded region. As shown by Figs. 17-19, the microhardness of the fusion zone shows a significant increase compared to the base metal outside the heat-affected zone in each of the three cases. However, there was no significant variation in fusion zone microhardness as a function of distance from the free surface of the weld. The microhardness increase in the heat-affected zone suggests that there was some oxygen pickup there, as well. A statistical analysis of the data in Figs. 17-19 is presented in Table VI. A similar microhardness analysis of laser-welded Ti-6Al-4V was reported (Ref. 10) in which the base metal was determined to have a comparable range of microhardness (335-350 Vickers Microhardness, load unspecified). However, the oxygen content of the fusion zone was reported to be 0.325% (presumably wt%) with a mean microhardness of ~380 VHN in an identical microstructure of 100% α' martensite. Whatever the source of these differences in correlation between dissolved oxygen measurement and degree of hardening in the fusion zone, the oxygen content observed here appears well within the range typical of Ti-6Al-4V ($\leq$0.3 wt%).

The narrow fusion zones of the specimens welded during this investigation precluded the preparation of tensile specimens with a gage length composed entirely of as-welded material. However, tensile specimens oriented perpendicular to welding direction were prepared from weld specimens 9 and 10, with the fusion zone placed in the center of the gage length (Fig. 5), and these were tested at ambient temperature. Additional data concerning the fusion zone yield strength was obtained by using two strain gages, one placed directly on the fusion zone and one on the material outside of the heat-affected zone. Thus the yield strength of the as-welded fusion zone, as well as that of the base metal, was obtained. These data are presented in Table VII, and two examples of the engineering stress-strain data from dual strain-gaged tensile specimens are shown in Figs. 20 and 21. The range of values of the fusion zone 0.2% yield stress was comparable to previous data from Ti-6Al-4V laser welds where the dissolved oxygen was reported to be higher (Ref. 10); and significantly lower than the data of another investigation which did not report a fusion zone oxygen content (Ref. 8). Overall, the tensile tests showed that the narrow gap/LAYERGLAZE welds were sound and were stronger than the unwelded plate. This strength differential is attributed both to the increased interstitial (oxygen) content of the fusion zone (Ref. 11), and to its finer microstructure; and is typical of welds in alpha-beta titanium alloys (Ref. 12). No evidence for fusion zone strengthening via martensite tempering (Ref. 12) during sequential layer deposition was observed by transmission electron microscopy (subsequently discussed).

The fracture toughness of weld specimens no. 9 and 10 were evaluated by fracturing Charpy specimens according to standard ASTM procedures (Ref. 13) (Table VIII). Apparently, the large prior-β grain size, which permitted the

formation of a substantial number of long plates (long undeviated crack paths) in the acicular α' resulted in a significant reduction in fracture energy compared to the normal range for solution annealed or solution annealed and aged Ti-6Al-4V (Ref. 14), an effect noted previously for similar microstructures formed by β-quenching (Ref. 15) and electron beam welding (Ref. 12). Examples of two of the force vs time curves recorded during these instrumented Charpy tests are shown in Fig. 22. Despite the relatively low fracture energies, these curves show that considerable plastic strain occurred during the fracture process. A higher range of fracture energies were obtained from another investigation of laser welded Ti-6-4 (Ref. 7), although the origin of this difference is not apparent as the microstructures are very similar.

C. Fusion Zone Microstructure

A detailed examination of the as-narrow-gap/Layerglazed microstructure shown in Figs. 13 and 14 was conducted by conventional metallography and analytical electron microscopy. As shown by Fig. 23, a grain structure typical of the LAYERGLAZE process was formed (Refs. 1-4), in which the grains grew epitaxially as each successive layer was deposited. By this means a coarse, columnar grain structure was formed in which the grains are aligned approximately parallel to the heat flux during solidification. Although this coarse grain structure might be interpreted as indicative of a relatively slow solidification rate, both a previously-published thermal analysis of fusion zone cooling rates in laser-welded titanium-base alloys (Ref. 16) and the fully martensitic microstructure which was observed strongly suggest that the solidification and solid state cooling rates in the narrow gap/LAYERGLAZE welds were $\geq 10^{4}$°C/s. Consequently, the fusion zones consisted entirely of α' HCP martensite, while the heat affected zone displayed a sharp microstructural gradient from all α' near the weld to finely mixed α+β near the base plate. A detailed view of this range of microstructures across the transverse section of a weld is shown in Figs. 24-26. The martensitic structures shown in Fig. 26 is somewhat deceptive, in that the very long α' plates which extend for hundreds of microns across the grains represent only the large end of the martensite plate size distribution. Examination of the fusion zone of specimen no. 9 by transmission electron microscopy (Fig. 27) revealed a much finer martensitic structure between these long plates, as the distance available for each new plate to form was successively reduced by those which had transformed earlier (geometric partitioning). Examination of relatively large amounts of this area, such as the ~$1.4(10^{3})\mu m^{2}$ shown in Fig. 27, confirmed that no grain boundary α was present in the fusion zone. At higher magnification, most of the microstructural characteristics previously reported in β-quenched Ti-6Al-4V were observed, although no evidence of retained β was detected (Ref. 17). Narrow stacking faults (Fig. 28) and longitudinally oriented $\{10\bar{1}1\}$ twins were visible within the larger plates, as well as the high dislocation

density characteristic of as-Layerglazed alloys (Refs. 1,2). Qualitative EDS and microdiffraction data obtained from STEM observation of the same specimen shown in Fig. 28 revealed no evidence of discrete grain boundary phases or chemical segregation (Fig. 29). However, the electron microscope was operated with a tungsten rather than a LaB_6 electron source, so that the spot intensity was not sufficient to reveal grain boundary segregation at the level of a monolayer or less.

Overall, the examination of narrow gap/LAYERGLAZE microstructure revealed no unexpected features. Although the grain structure was large and columnar, the martensitic structure within the grains was homogeneous and contained a very wide range of α' HCP martensite plate lengths (<1μm to >100μm). No phase distribution or chemical segregation unique to the grain boundaries could be observed, and the dislocation density appeared to be high enough to permit recrystallization of the fusion zone, should this prove desirable.

CONCLUSIONS

1. The powder-feed LAYERGLAZE Process can be used to make sound, narrow, 4 mm straight-sided gap welds in 1.7 and 2.5 cm thick Ti-6Al-4V plate.

2. Preplaced feedstock of solution blend Ti-6Al-4V powder can be used to form narrow-gap welds with mechanical properties comparable to close-fitting laser butt welds in Ti-6Al-4V plate.

3. Narrow gap welds in Ti-6Al-4V plate can be made by Layerglazing with continuous powder feed, but improved beam control to eliminate premature sidewall fusion above the gap floor will be required to avoid sidewall bridging and consequent macroscopic cavities.

4. The fusion zone cooling rate was sufficiently rapid ($\geq 10^4$ °C/s) so that the resulting microstructure was entirely composed of acicular α' HCP martensite, with no formation of grain boundary α.

5. The high dislocation density and phase metastability inherent in Layerglazed Ti-6Al-4V welds would allow the improvement of fusion zone fracture toughness by post weld heat treatment to induce grain refinement through recrystallization and fine-scale β precipitation.

6. No evidence for interdendritic or grain boundary segregation of elements with Z >10 could be detected in the fusion zone by TEM/STEM EDS analysis.

REFERENCES

1. E. M. Breinan, D. B. Snow and C. O. Brown: Program to Investigate Advanced Laser Processing of Materials, UTRC Final Report R81-914346-8, Contract N00014-78-C-0387, ARPA Order No. 3542, Jan. 1981.

2. E. M. Breinan, D. B. Snow, C. O. Brown and B. H. Kear: New Developments in Laser Surface Melting Using Continuous Prealloyed Powder Feed, Rapid Solidification Processing, Principles and Technologies, II, R. Mehrabian, B. H. Kear and M. Cohen, eds., Claitor's Publishing Div., Baton Rouge, 1980, p 440.

3. B. H. Kear, J. W. Mayer, J. M. Poate, and P. R. Strutt: Surface Treatments Using Laser, Electron and Ion Beam Processing Methods, Metallurgical Treatises, J. K. Tien and J. F. Elliott, eds., TMS-AIME, Warrendale, PA, 1981, p 321.

4. L. M. Masur, E. M. Breinan and C. O. Brown: Application of the LAYERGLAZE Process to JT-8D Turbine Spacer Knife Edge Seal Repair, UTRC Report R79-210405-1, August 1979.

5. E. M. Breinan and C. M. Banas: Fatigue of Laser-Welded Ti-6Al-4V, UTRC Report R75-412260-1, July 1975.

6. W. A. Baeslack III and C. M. Banas: A Comparative Evaluation of Laser and Gas Tungsten Arc Weldments in High Temperature Titanium Alloys, J. Welding, 60, 121s-130s (1981).

7. F. W. Fraser and E. A. Metzbower: Laser Welding of a Titanium Alloy, Advanced Processing Methods for Titanium, D. F. Hasson and C. H. Hamilton, eds., TMS-AIME, Warrendale, PA, 1982, p 175.

8. T. C. Peng, S. M. L. Sastry, J. E. O'Neal and J. F. Tesson: Microstructures and Mechanical Properties of Laser-Welded Titanium Alloys, ibid., p 189.

9. Y. Arata: Narrow Gap High Energy Beam Welding (1) - Principle, Trans. Japan Welding Institute, 2, 119-120 (1973).

10. J. Mazumder and W. M. Steen: Microstructure and Mechanical Properties of Laser Welded Titanium 6Al-4V, Met. Trans. A, 13A, 865-71 (1982).

11. K. Shimasaki, K. Ono, and T. Tsuruno: Relation Between Brinell Hardness of Titanium and Impurities (O_2,Fe,N, and C), Titanium '80, Science and Technology, H. Kimura and O. Izumi, eds., TMS-AIME, Warrendale, PA, 1980, p 1131.

12. D. W. Becker, R. W. Messler, Jr. and W. A. Baeslack III: Titanium Welding - A Critical Review, ibid., p 256.

13. 1981 Annual Book of ASTM Standards, Part 10, Section E23-81, ASTM, Philadelphia, 1981.

14. H. Margolin, J. C. Williams, J. C. Chesnutt and G. Luetjering: A Review of the Fracture and Fatigue Behavior of Ti Alloys, Titanium '80, Science and Technology, H. Kimura and O. Izumi, eds., TMS-AIME, Warrendale, PA, 1982, p 169.

15. M. Ashraf Imam and C. M. Gilmore: New Observations of the Transformations in Ti-6Al-4V, ibid., p 1534.

16. T. C. Peng, S. M. L. Sastry and J. E. O'Neal: Exploratory Study of Laser Processing of Titanium Alloys, Lasers in Metallurgy, K. Mukerjee and J. Mazumder, eds., TMS-AIME, Warrendale, PA, 1981, p 279.

17. J. C. Williams and M. J. Blackburn: A Comparison of Phase Transformations in Three Commercial Titanium Alloys, TASM, 60, 373-83 (1967).

Table I

Ti-6Al-4V Powder Feedstock Specifications

Powder Type	Mesh Size Range (as-received)	Source
Mechanically Blended Elemental	-170, +325	Amerimet Simsbury, CT
Prealloyed	-35, +325	Nuclear Metals Concord, MA

Table II

Composition of Prealloyed Ti-6Al-4V Powder Feedstock
(supplied by manufacturer)

Element:	Al	V	Fe	W	Cu	O	N	C	H_2
wt%	6.6	4.2	0.16	0.0007	0.0027	0.173	0.012	0.012	0.0036

Table III

Summary of Welding Parameters, Initial Series of Ti-6Al-4V Specimens

Specimen Identification Number	Plate Thickness (cm)	Laser Power at Specimen Surface(kW)	Speed (cm/min)	Powder Type	Gap (mm)	Comments
3	1.27	3.9	127	Mechanical blend and prealloyed	3.0	Initial specimen. Test interrupted by work station breakdown. Switched from mechanical to solution blend powder. Specimen lowered 0.25 mm every 2 passes.
4	1.27	3.9	127	Prealloyed	4.1	57 passes in 7.41 minutes. Specimen lowered 1 mm every 4 passes.
5	2.54	3.9	127	Prealloyed	4.1	Step at bottom of gap. ~100 passes Buildup was ~0.25 mm/pass. Specimen lowered 1 mm every 4 passes.
6	2.54	3.9	127	Prealloyed	4.1	Step at center line of plate. Top section ~50 passes. Powder built up in groove in one section. Run stopped then restarted. Second side. Gap closed down to ~2.5 mm to begin. Specimen lowered 1 mm every 4 passes.

Table IV

Summary of Welding Parameters, Second Series of Ti-6Al-4V Specimens

Specimen Identification Number	Plate Thickness (cm)	Laser Power at Specimen Surface (kW)	Speed (cm/min)	Powder Type	Gap (mm)	Comments
7	2.54	3.9-5.1	127	Prealloyed	4.2	Rotating focusing mirror. Top of gap bridged in 3 places when 5.1 kW used. No pass completed.
8	2.54	3.9	127	Prealloyed	4.2	47 cm focal length, stationary mirror. Gap randomly bridged by powder.
9	2.54	3.9	51	Prealloyed	4.2	Spot diameter << gap width. Powder preplaced before each pass.
10	2.54	3.9	51-127	Prealloyed	4.2	Powder preplaced before each pass. Welding terminated at one-half depth by specimen warpage and consequent gap closure.

Table V

Chemical Analysis, Weld Specimen No. 9

Element (Wt%):	Al	W	O
Base metal, weld no. 9	6.1	4.1	0.11
Fusion zone, weld no. 9			0.14

Table VI

Analysis of Microhardness Data, Weld Specimen No. 9

		Sample Size	Mean DPH	Unbiased Standard Deviation
UPPER SECTION	Base Metal*	10	355	14
	Fusion Zone	17	414	13
MIDDLE SECTION	Base Metal*	10	341	29
	Fusion Zone	16	418	9
LOWER SECTION	Base Metal*	10	330	16
	Fusion Zone	16	419	20
OVERALL	Base Metal*	30	342	23
	Fusion Zone	49	417	14

Table VII

Tensile Test Data, Weld Specimens No. 9 and 10

Weld Specimen	Identification	Weld Strain Gage 0.2% YS MPa(ksi)	Unwelded Zone Strain Gage 0.2% YS MPa(ksi)	Unwelded Zone Strain Gage UTS MPa(ksi)	% ε Fusion + Unwelded Zones
9	- *	-	841(122)	874(127)	12.3
9	9C-2**	>883(128)	800(116)	862(125)	9.9[1]
9	9F-2**	834(121)	807(117)	855(124)	10.7[1]
9	9H-1**	855(124)	800(116)	869(126)	10.8[1]
9	9C-1	-	-	862(125)	10.6[1]
9	9D-1	-	-	848(123)	9.1[1]
9	9D-2	-	-	855(124)	9.4[1]
9	9F-1	-	-	807(117)	1.1[2]
9	9H-2	-	-	862(125)	9.5[1]
10	10B-2**	821(119)	800(116)	876(127)	9.0[1]
10	10D-2**	>848(123)	793(115)	848(123)	9.7[1]
10	10B-2	-	-	862(125)	10.8[1]

*as-received only, no weld, average of four tests
**separate strain gages, fusion and unwelded zones

[1] failure in unwelded zone
[2] failure in fusion zone, macroscopic internal porosity

Table VIII

Ambient Temperature Fracture Toughness Data,
Weld Specimens No. 9 and 10

Weld Specimen	Identification	Measured 1/2 - Size Charpy V-Notch Energy Joules(ft-lb)	Calculated Full Size Charpy V-Notch Energy Joules(ft-lb)
9	9A-1	5.55(4.09)	11.61(8.65)
9	9A-2	5.94(4.38)	12.19(8.99)
9	9B-1	5.02(3.70)	10.78(7.95)
9	9B-2	5.94(4.38)	12.38(9.13)
9	9B-3	4.83(3.56)	14.51(10.7)
9	9B-4	4.23(3.12)	8.65(6.38)
9	9E-1	11.81(8.71)	24.14(17.8)
9	9E-2	6.24(4.60)	12.95(9.55)
10	10A-2	4.01(2.96)	8.45(6.23)
10	10A-3	4.77(3.52)	9.89(7.29)
10	10C-1	4.46(3.29)	9.21(6.79)

NARROW GAP WELD SPECIMEN CONFIGURATIONS

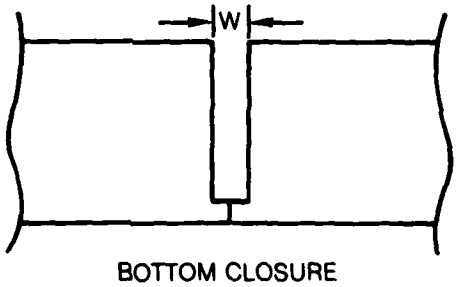

BOTTOM CLOSURE
W = 0.31 — 0.46 cm

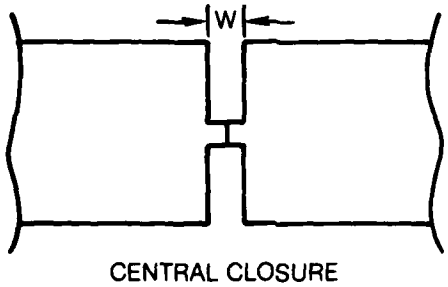

CENTRAL CLOSURE
W = 0.31 — 0.46 cm

NARROW GAP WELD POSITIONING FIXTURE

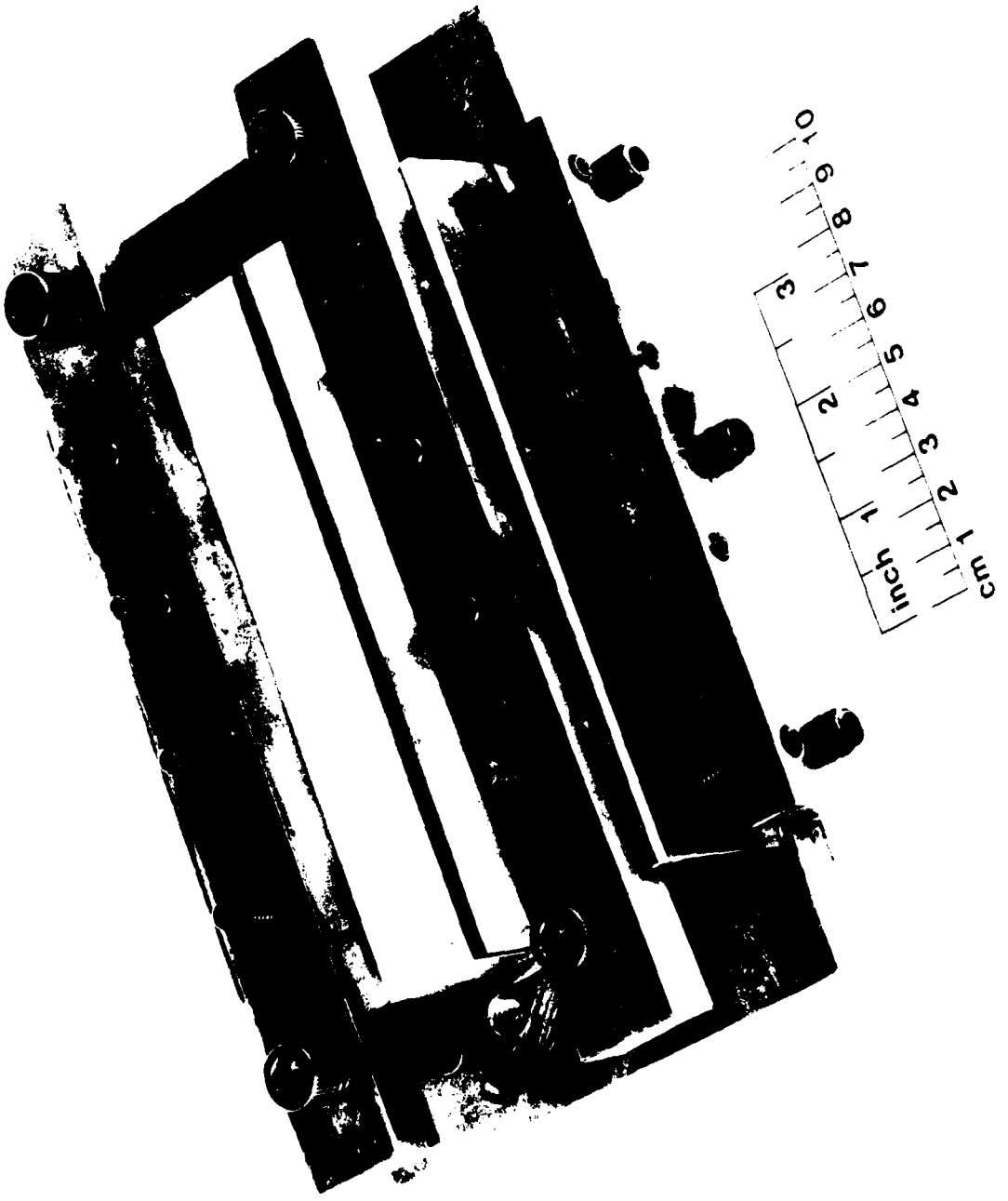

PROTECTIVE ATMOSPHERE CHAMBER FOR TITANIUM/NARROW-GAP LASER WELDING CHAMBER CLOSED AND POSITIONED ON 3 AXIS "SLO-SYN" MILLING TABLE

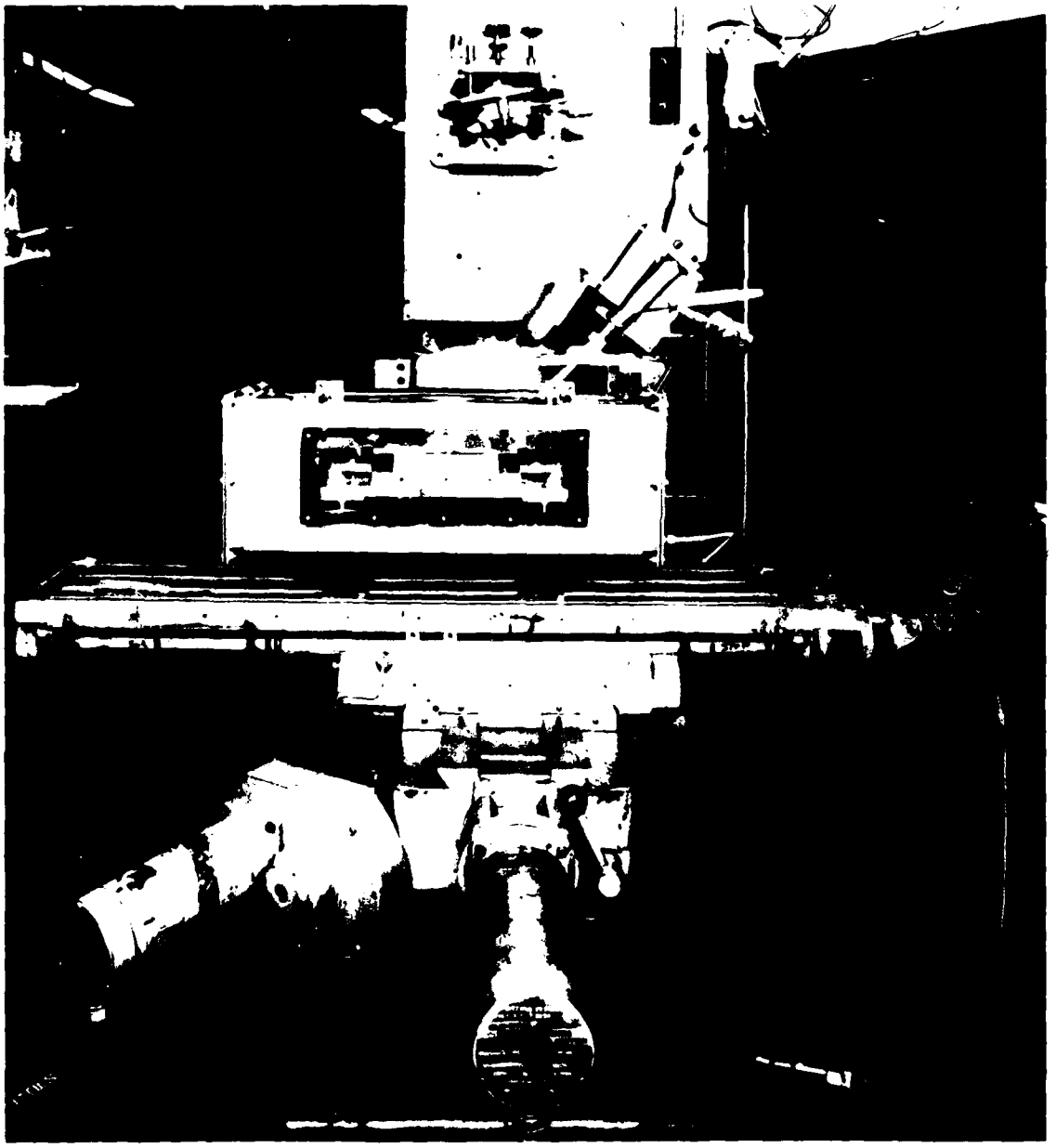

PROTECTIVE ATMOSPHERE CHAMBER FOR TITANIUM/NARROW-GAP WELDING

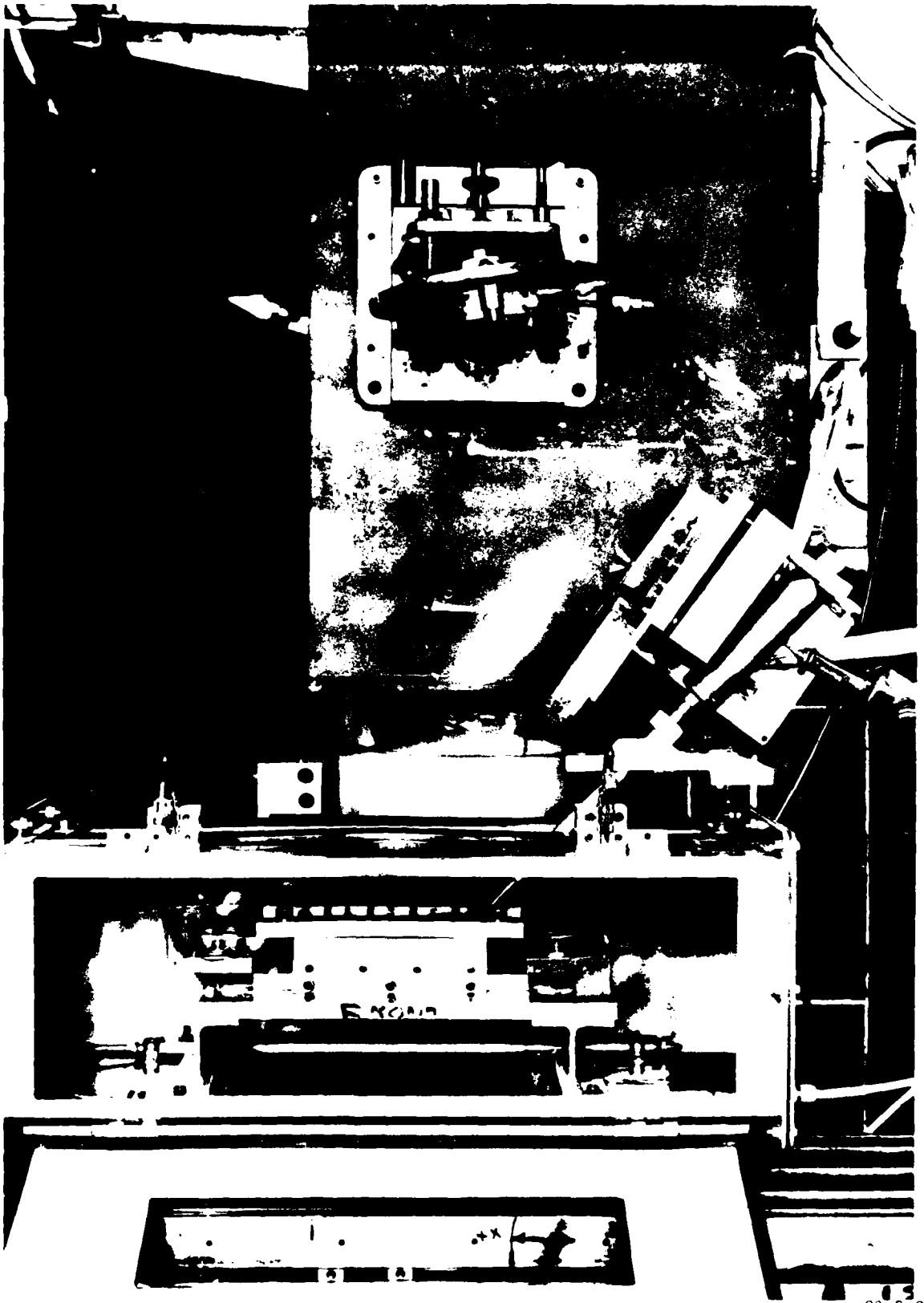

81-448 8

82 8 94 12

LOCATION OF MECHANICAL TEST SPECIMENS IN WELD SAMPLE SLICES

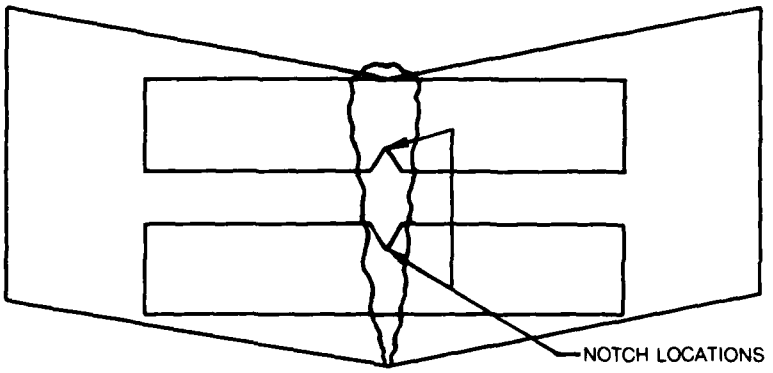

CHARPY IMPACT SPECIMENS

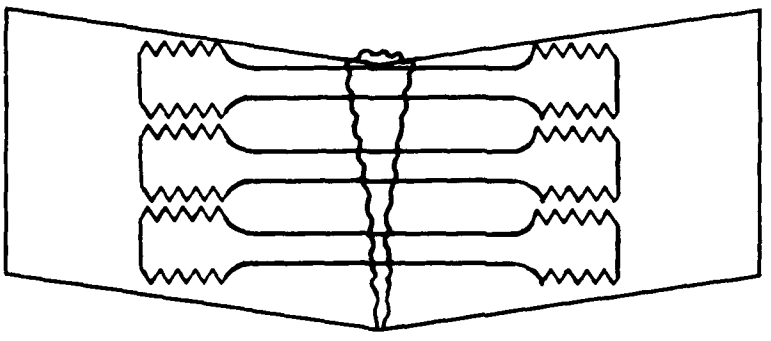

CROSS-WELD TENSILE SPECIMENS

NARROW GAP WELD SPECIMEN NO. 3

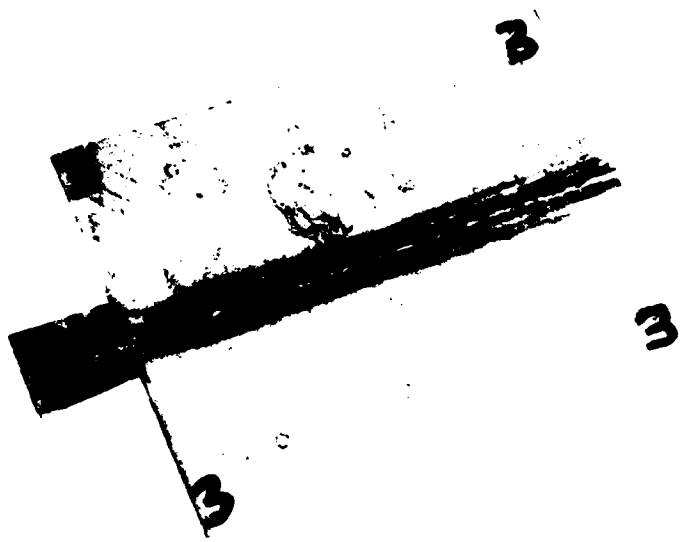

NARROW GAP WELD SPECIMEN NO. 4

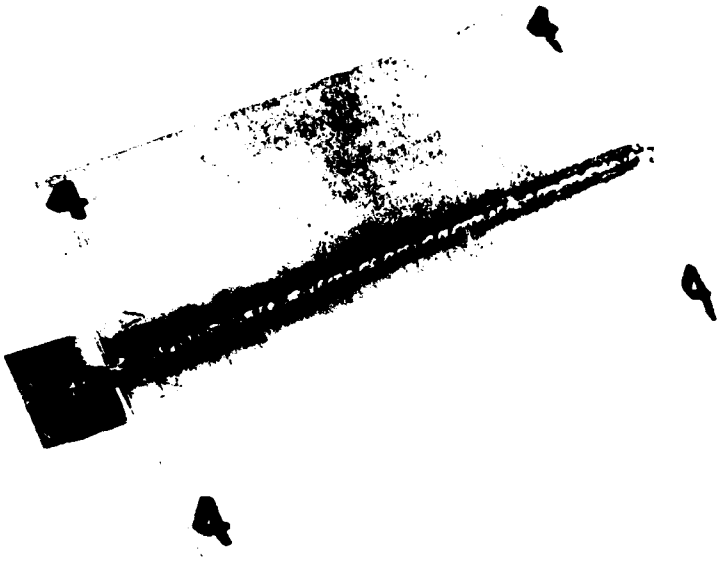

MACRO PHOTOGRAPH

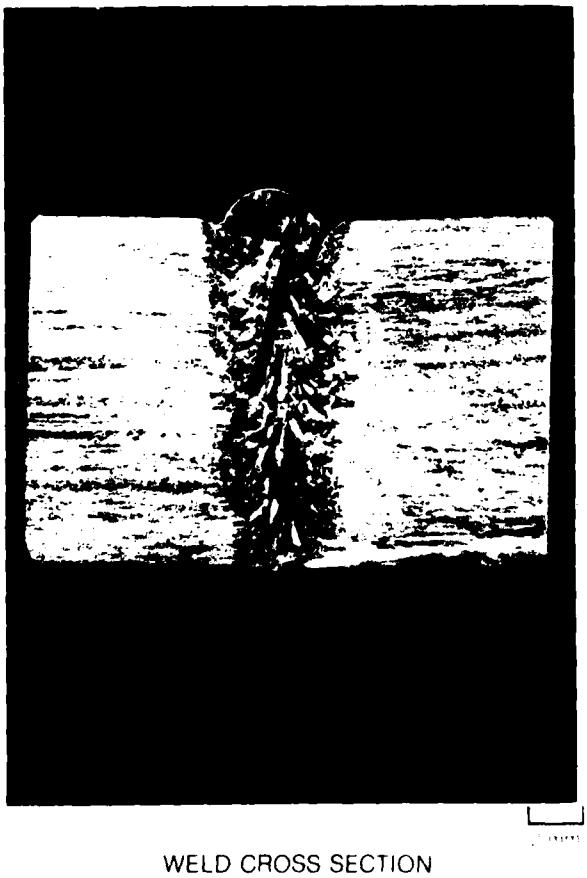

WELD CROSS SECTION

TYPICAL FLAW

82 8 94 10

NARROW GAP WELD SPECIMEN NO. 5

TOP VIEW

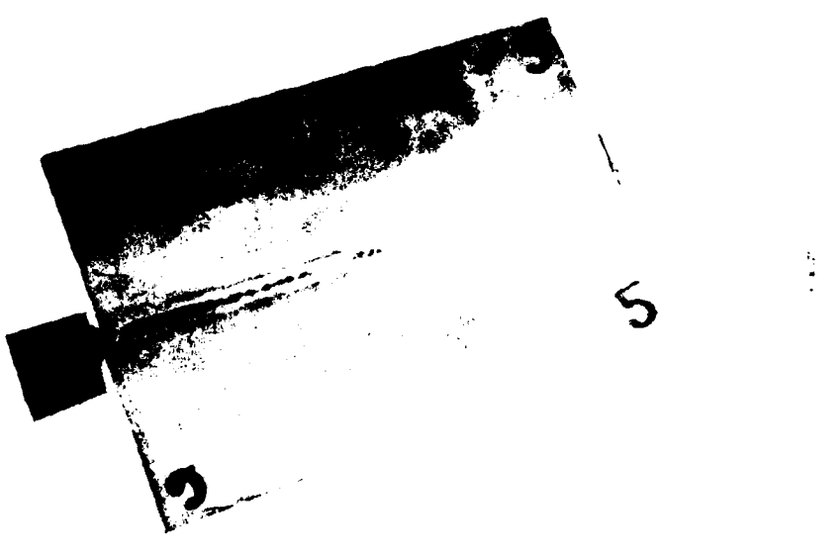

BOTTOM VIEW

R82-915797-2

MICROSTRUCTURE OF CROSS SECTION AND TYPICAL FLAW IN WELD NO. 5

CROSS SECTION

DETAIL OF LACK OF FUSION IN
BOTTOM CORNER OF WELD

82-8-94-1

FIG. 9

NARROW GAP WELD SPECIMEN NO. 6

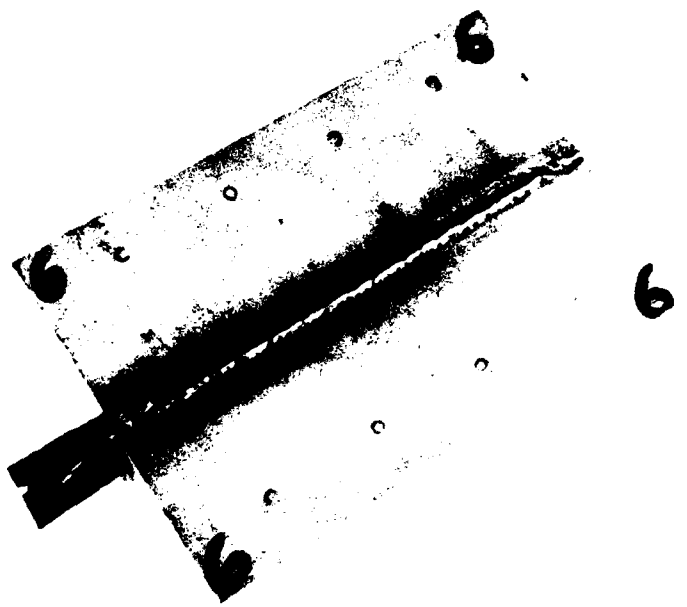

TOP VIEW

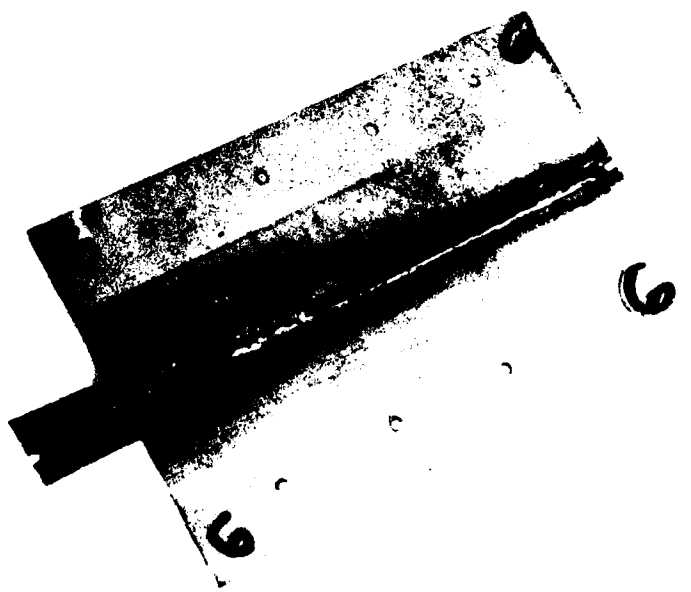

BOTTOM VIEW

FIG. 11

MICROSTRUCTURE OF CROSS SECTION AND DETAIL OF SMALL FLAW IN WELD NO. 6

MACROPHOTOGRAPH OF CROSS SECTION

SMALL FLAW NEAR ONE ROOT

SOUND WELD MICROSTRUCTURE

82-8-94-4

FIG. 12

MACRO-VIEW AND CROSS SECTION OF NARROW GAP WELD NO. 8

(NOTE EFFECT OF SIDE-TO-SIDE BRIDGING)

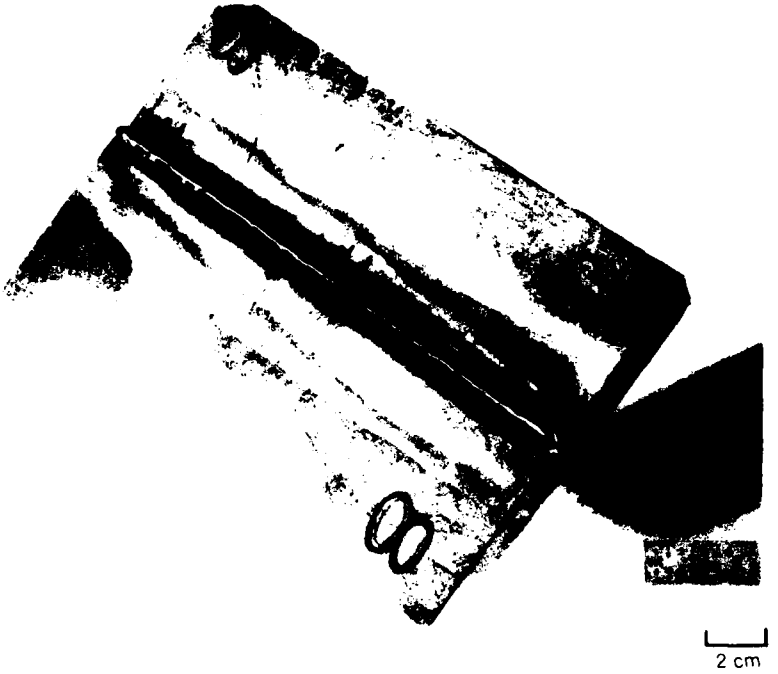

MACRO PHOTOGRAPH

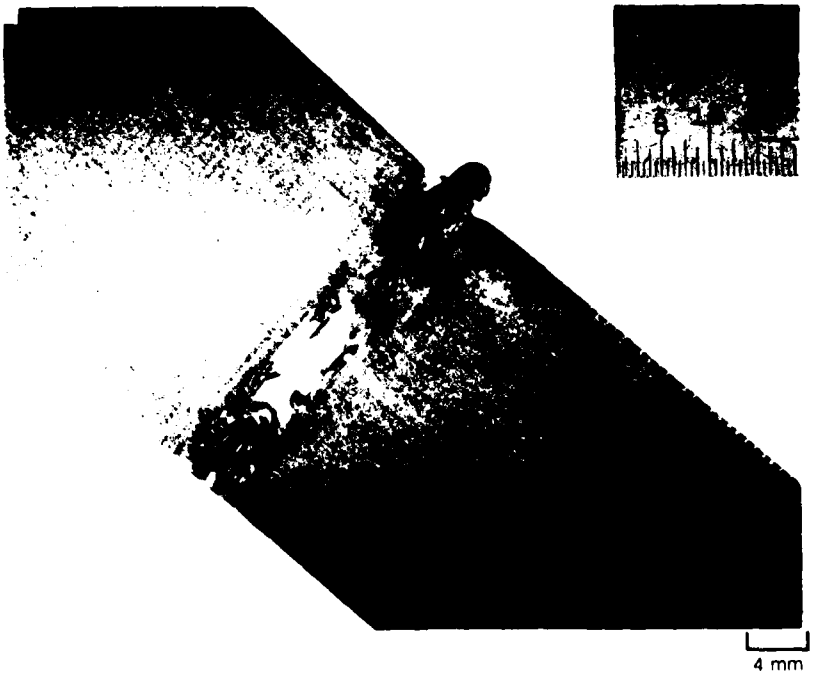

CROSS SECTION OF WELD

82-8-94-5

NARROW GAP WELD SPECIMEN NO. 9

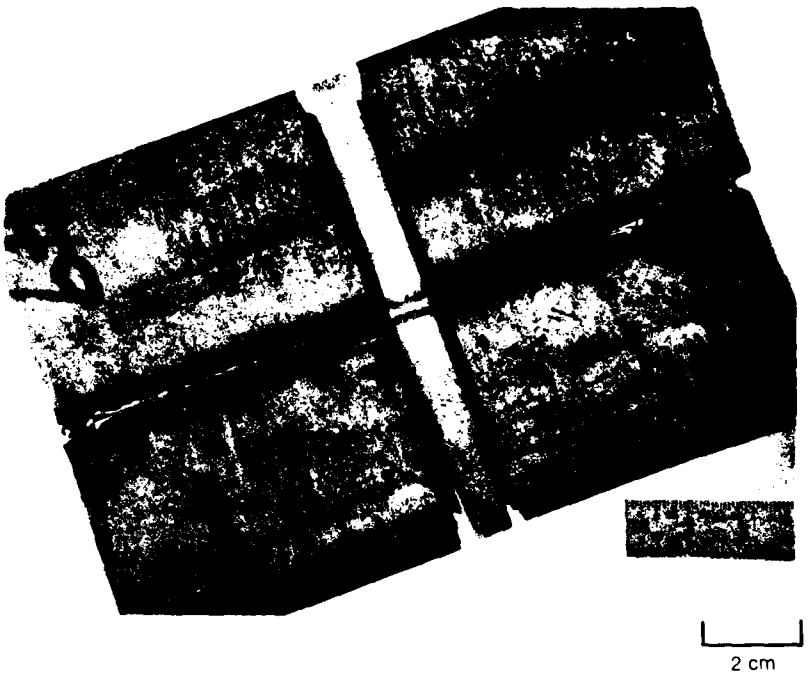

MACRO PHOTOGRAPH

TRANSVERSE MICROSTRUCTURE

INTERLAYER POROSITY, WELD NO. 9

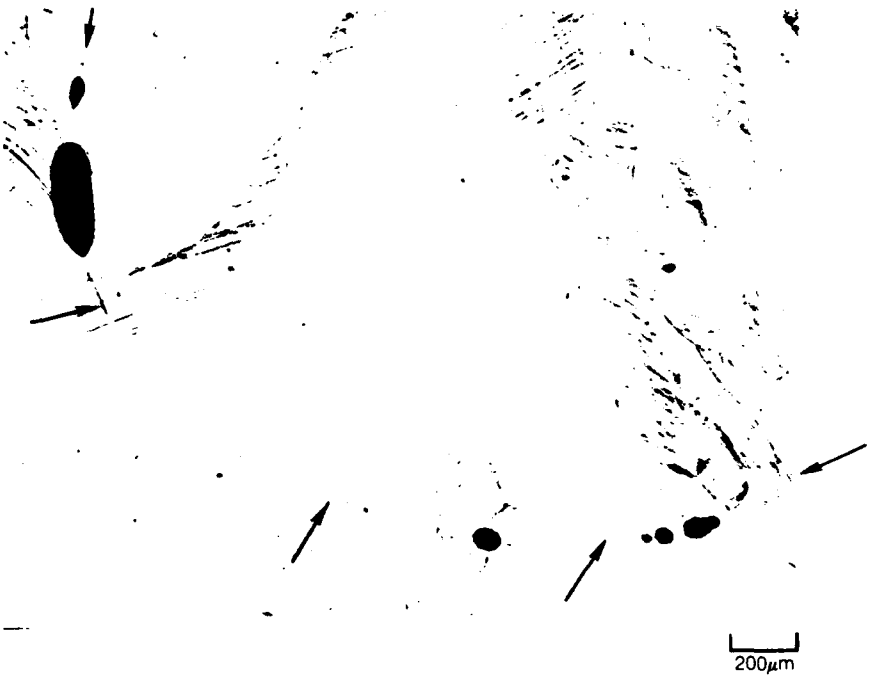

(ARROWS SHOW LAYER INTERFACE)

NARROW GAP WELD SPECIMEN NO. 10

MACRO PHOTOGRAPH

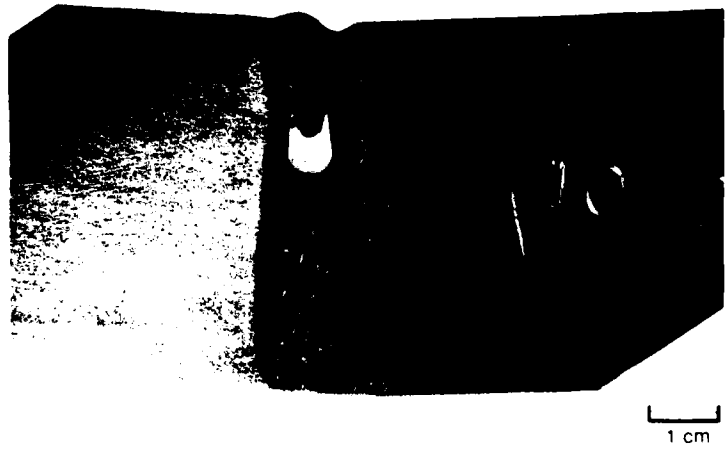

TRANSVERSE MICROSTRUCTURE

INTERLAYER POROSITY, WELD NO. 10

(ARROWS SHOW OCCASIONAL SMALL SPHERICAL VOIDS AT INTERFACE BETWEEN PASSES)

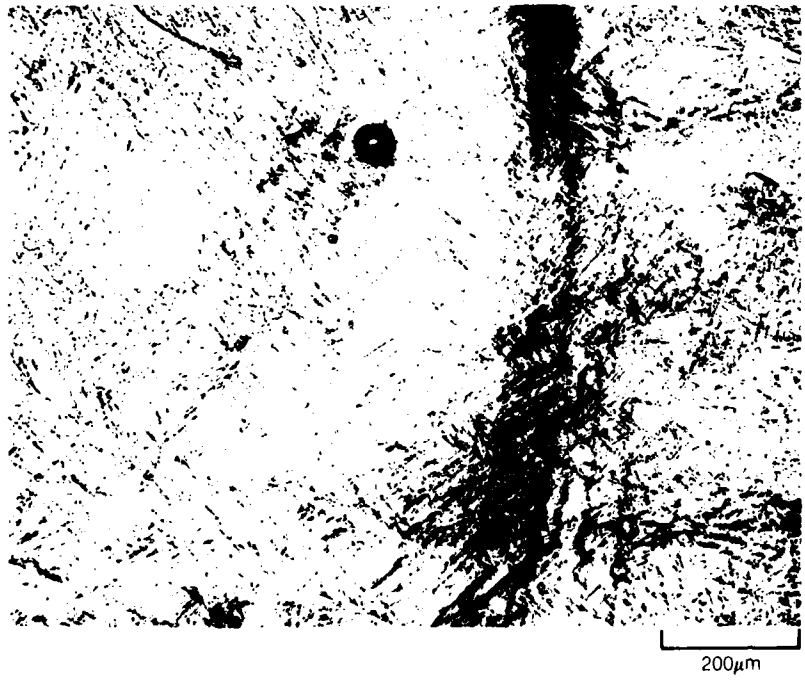

82-8-94-9

TRANSVERSE MICROHARDNESS SCAN — WELD NO. 9

UPPER SECTION

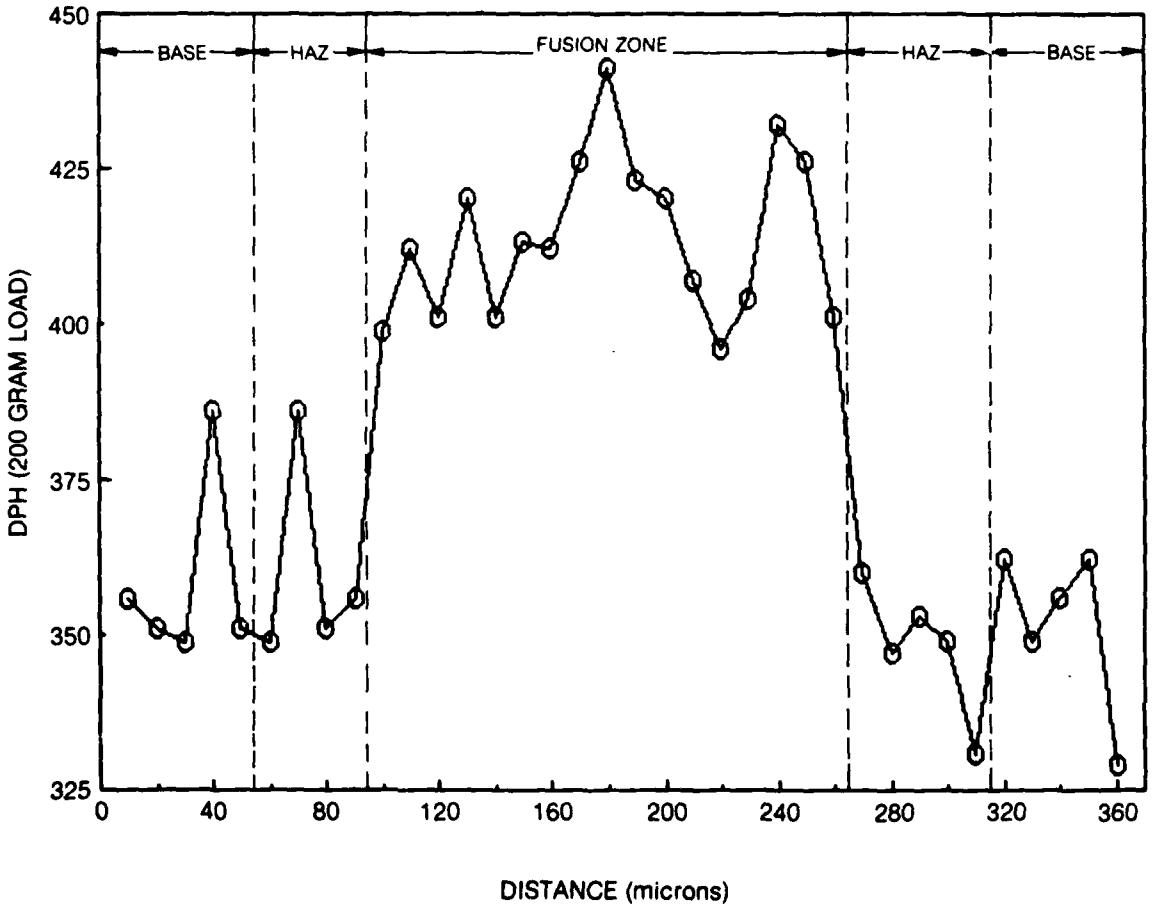

82-8-94-19

TRANSVERSE MICROHARDNESS SCAN — WELD NO. 9

MIDDLE SECTION

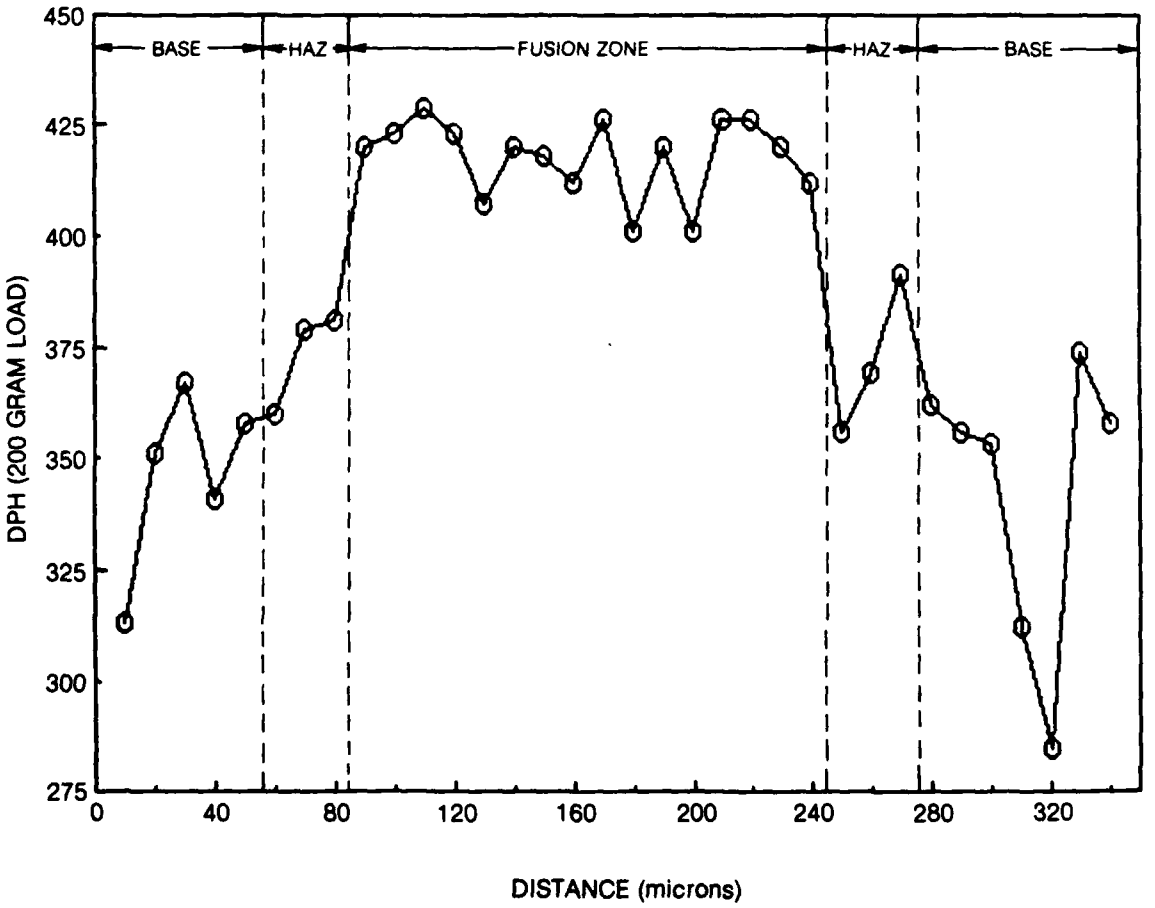

82-8-94-18

TRANSVERSE MICROHARDNESS SCAN — WELD NO. 9

LOWER SECTION

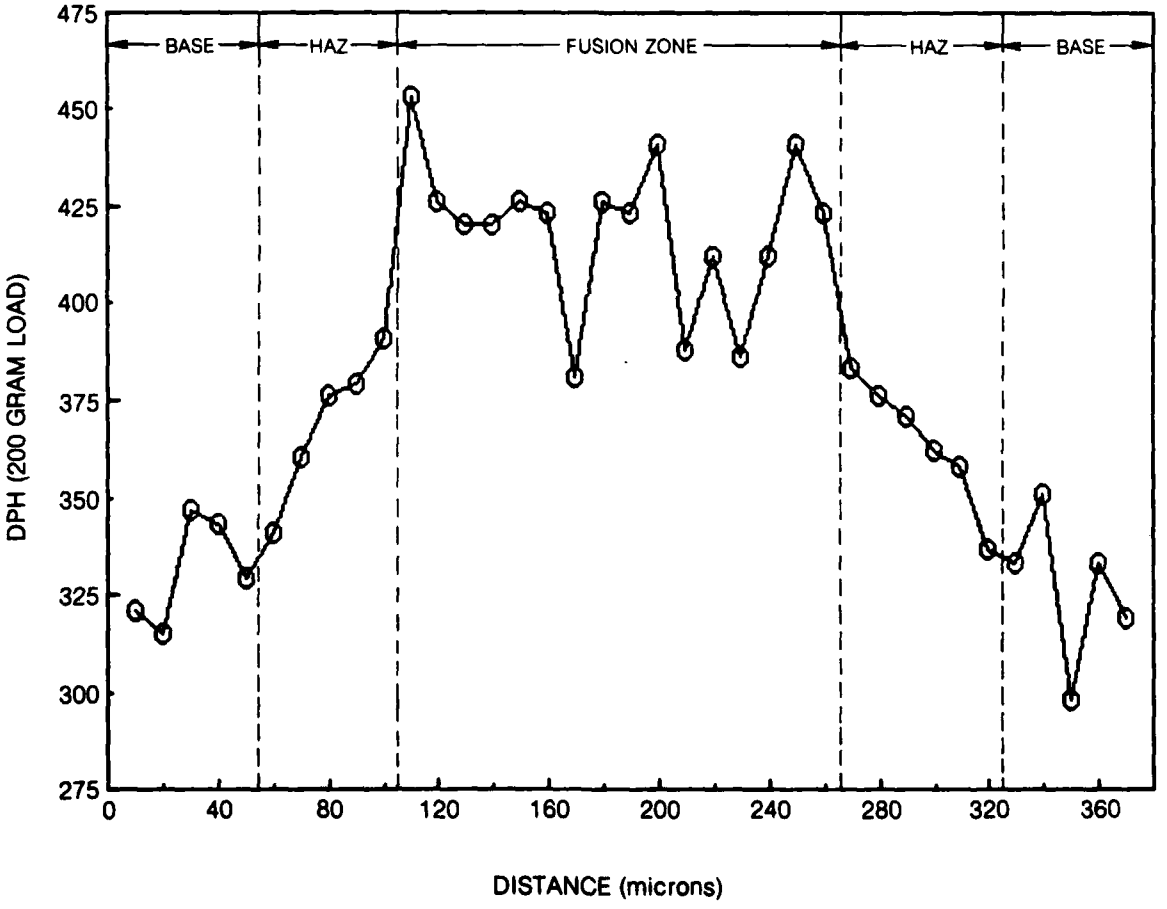

82-8-94-17

FIG. 20

STRESS VS STRAIN

WELD SPECIMEN NO. 9, AMBIENT TEMPERATURE, SAMPLE #9C-2

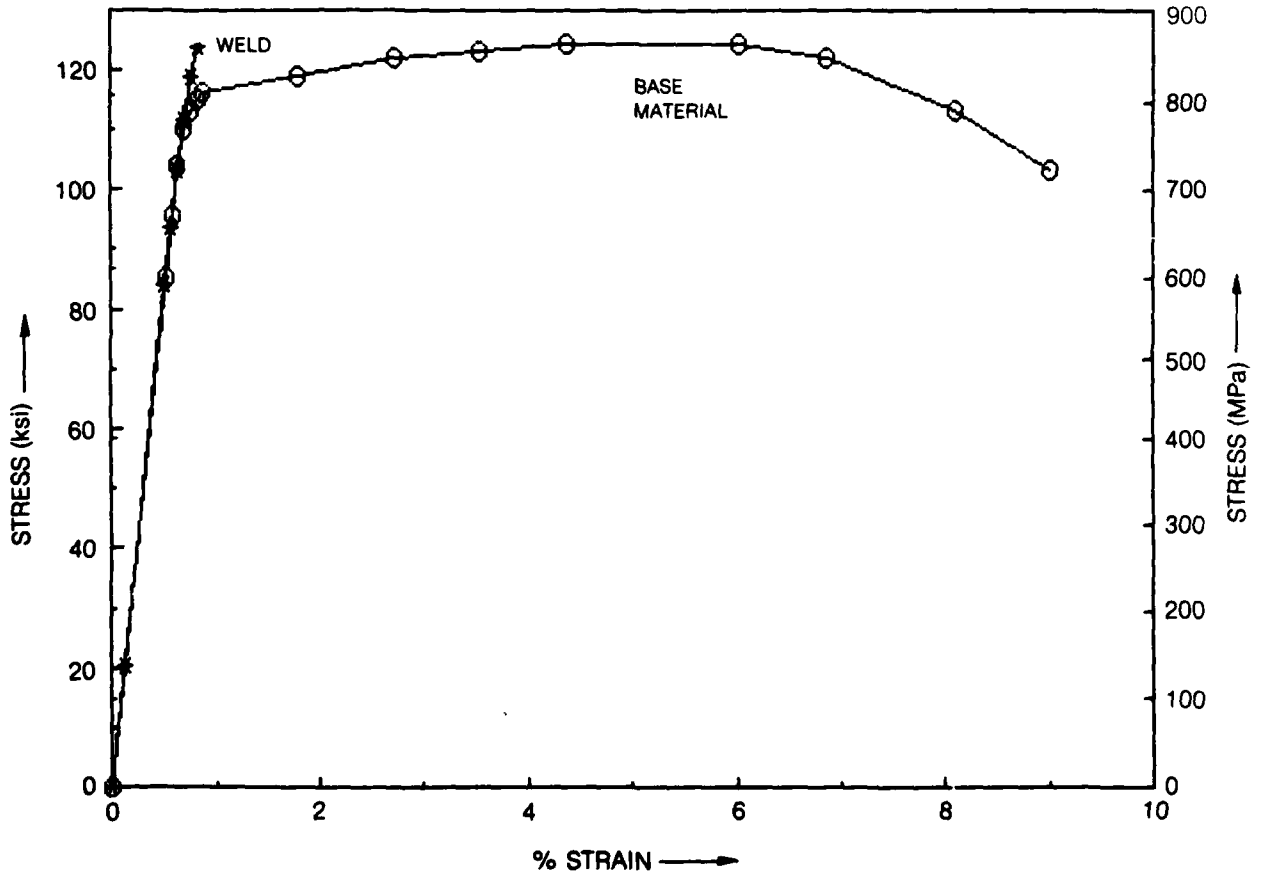

82-8-94-26

FIG. 21

STRESS VS STRAIN

WELD SPECIMEN NO. 10, AMBIENT TEMPERATURE, SAMPLE #10B-2

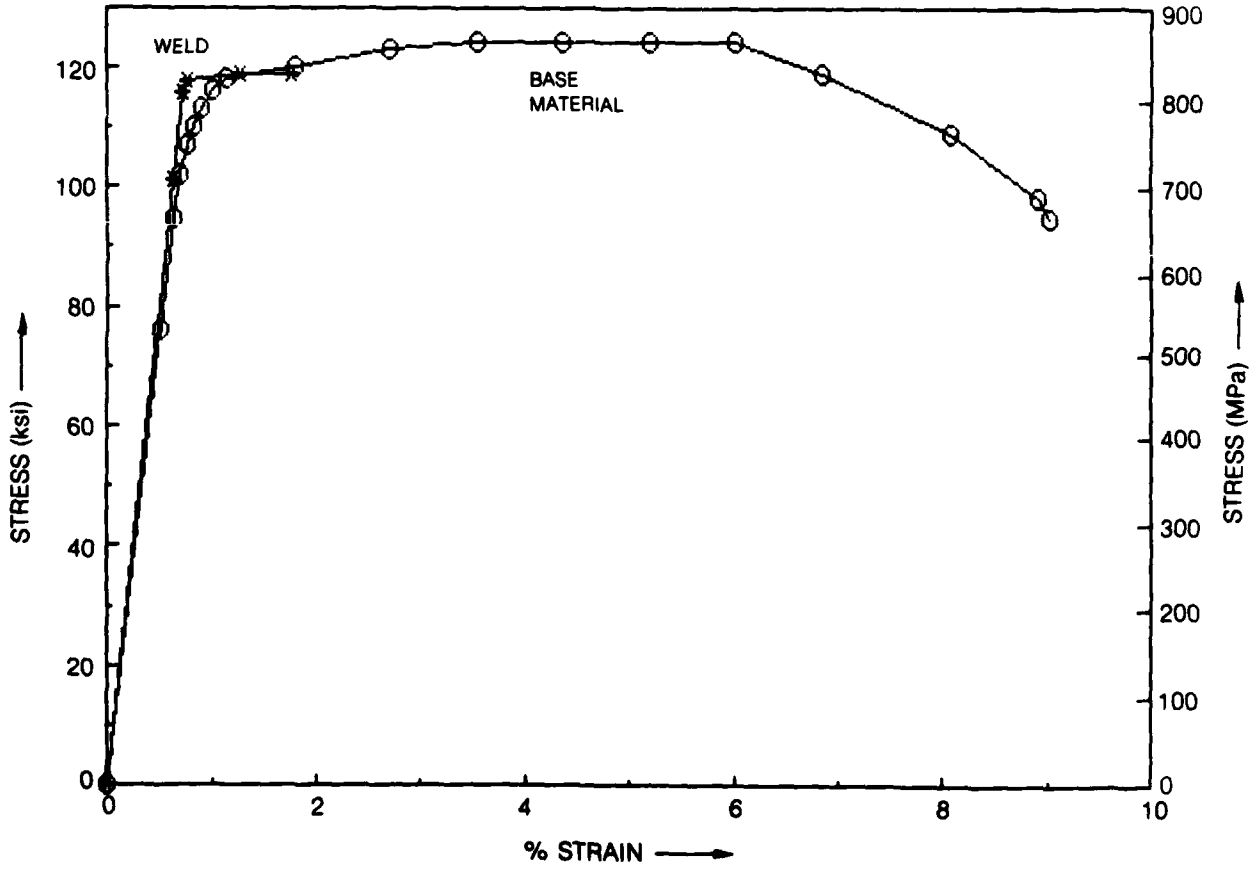

82-8-94-25

FORCE-TIME DATA, FUSION ZONE HALF-SIZE CHARPY IMPACT SPECIMENS

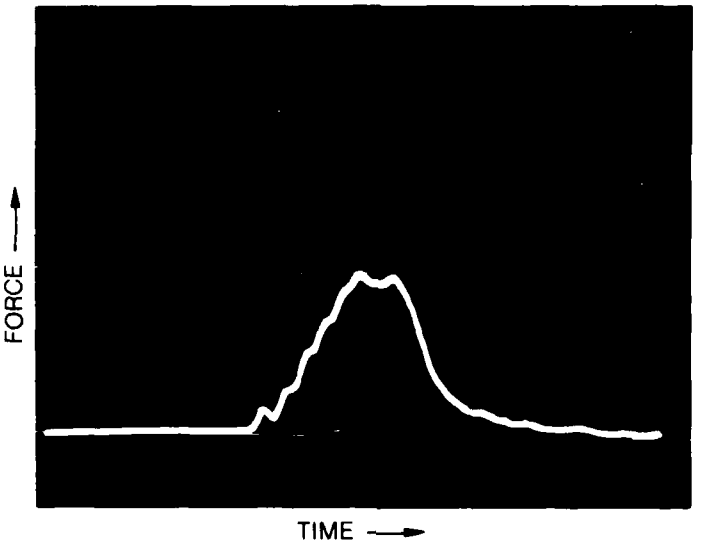

(a) SPECIMEN 9A-1, WELD NO. 9, AMBIENT TEMPERATURE

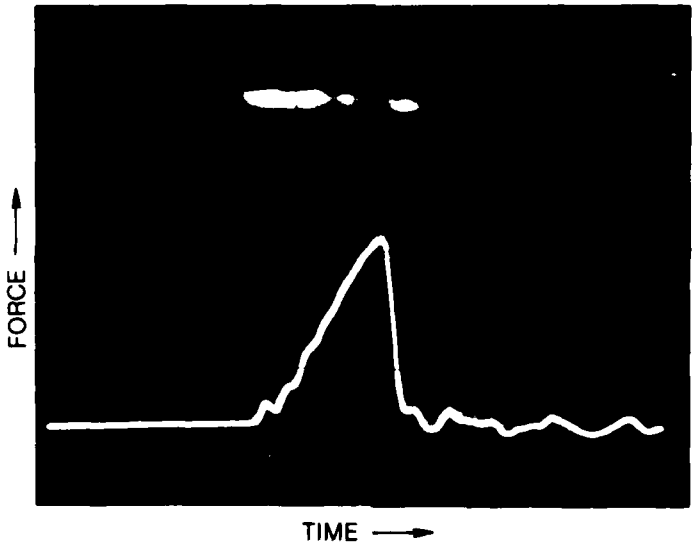

(b) SPECIMEN 10A-2, WELD NO. 10, AMBIENT TEMPERATURE

TOP

GRAIN STRUCTURE-LAYERGLAZE/NARROW GAP WELD SPECIMEN NO. 9

(OVERVIEW OF ENTIRE WELD)

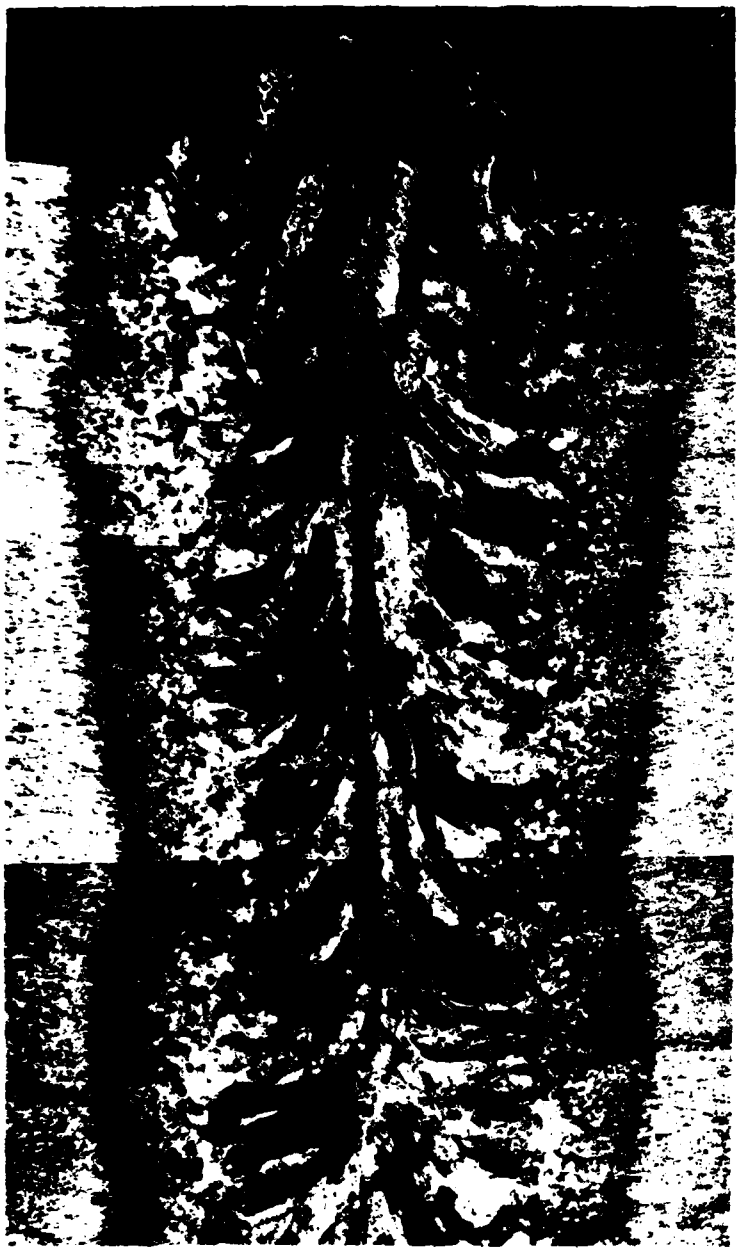

BOTTOM

0.8mm

82-8-94-23

R82-915797-2

FIG. 23

FIG. 24

GRAIN STRUCTURE — LAYERGLAZE/NARROW GAP WELD SPECIMEN NO. 9

(VARIATION IN MICROSTRUCTURE ACROSS WELD)

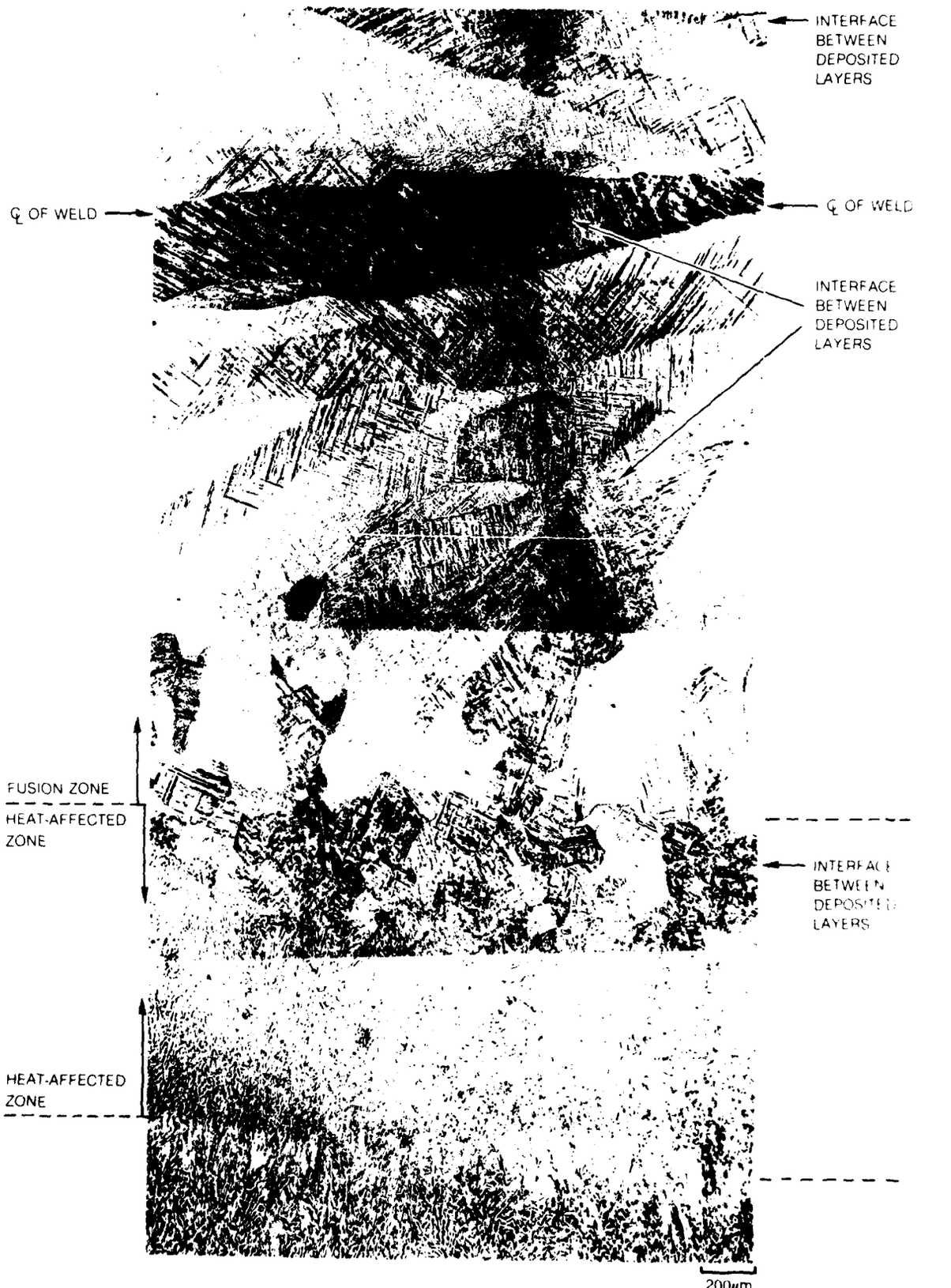

FIG. 25

GRAIN STRUCTURE — LAYERGLAZE/NARROW GAP WELD SPECIMEN NO. 9

(ENLARGED VIEW OF MICROSTRUCTURE)

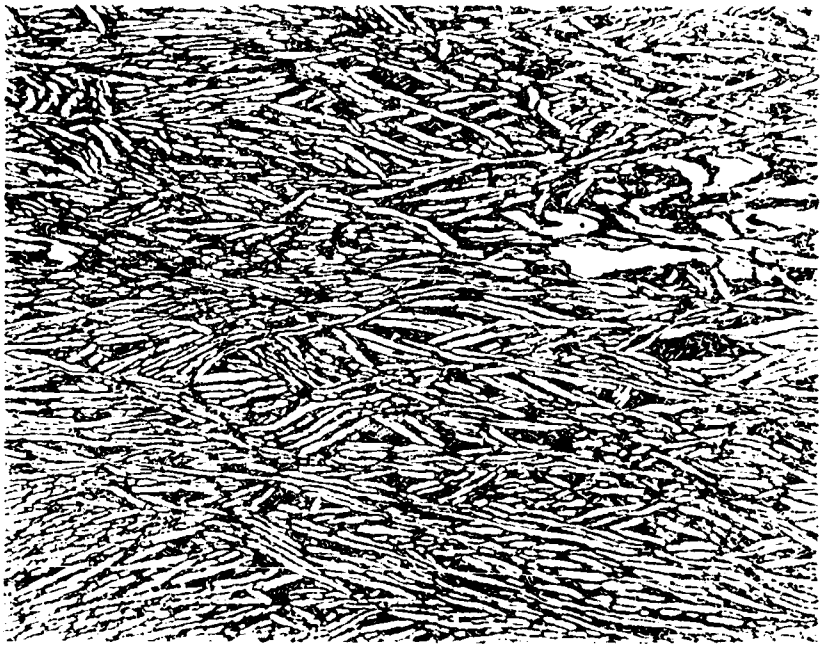

a) AS-RECEIVED; OUTSIDE OF WELDED REGION

50μm

b) HEAT-AFFECTED ZONE, NEAR FUSION ZONE

50μm

82-8-94-20

FIG. 26

GRAIN STRUCTURE-LAYERGLAZE/NARROW GAP WELD SPECIMEN NO. 9

(ENLARGED VIEW OF MICROSTRUCTURE)

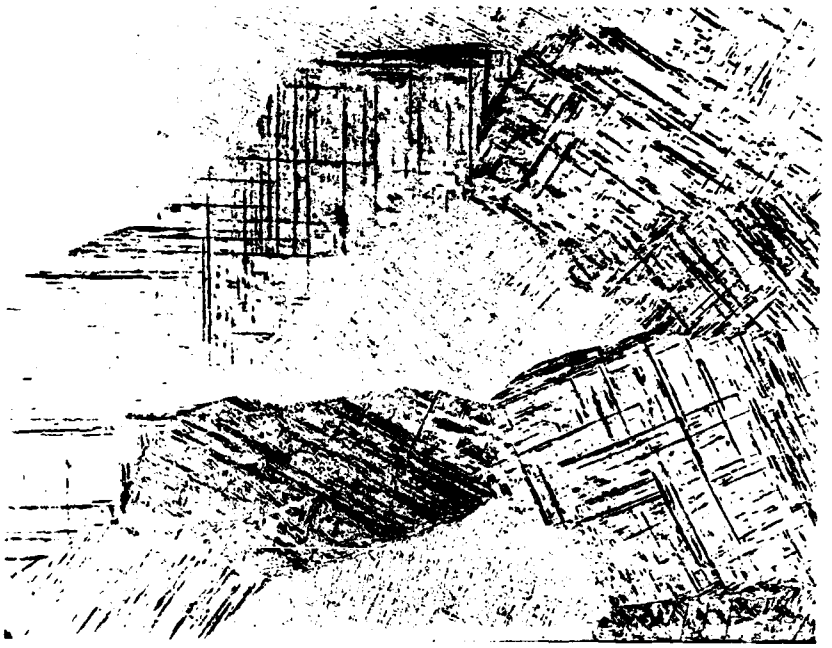

a) FUSION ZONE, NEAR HEAT-AFFECTED ZONE

50μm

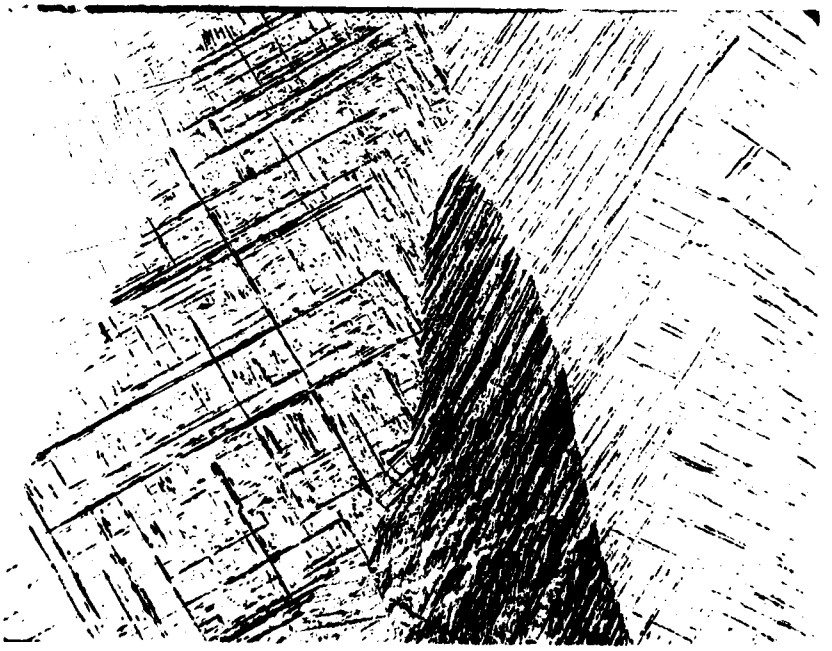

b) FUSION ZONE, NEAR CENTER LINE OF WELD

50μm

82-8-94-22

FIG 27

α' HCP MARTENSITIC STRUCTURE OF FUSION ZONE

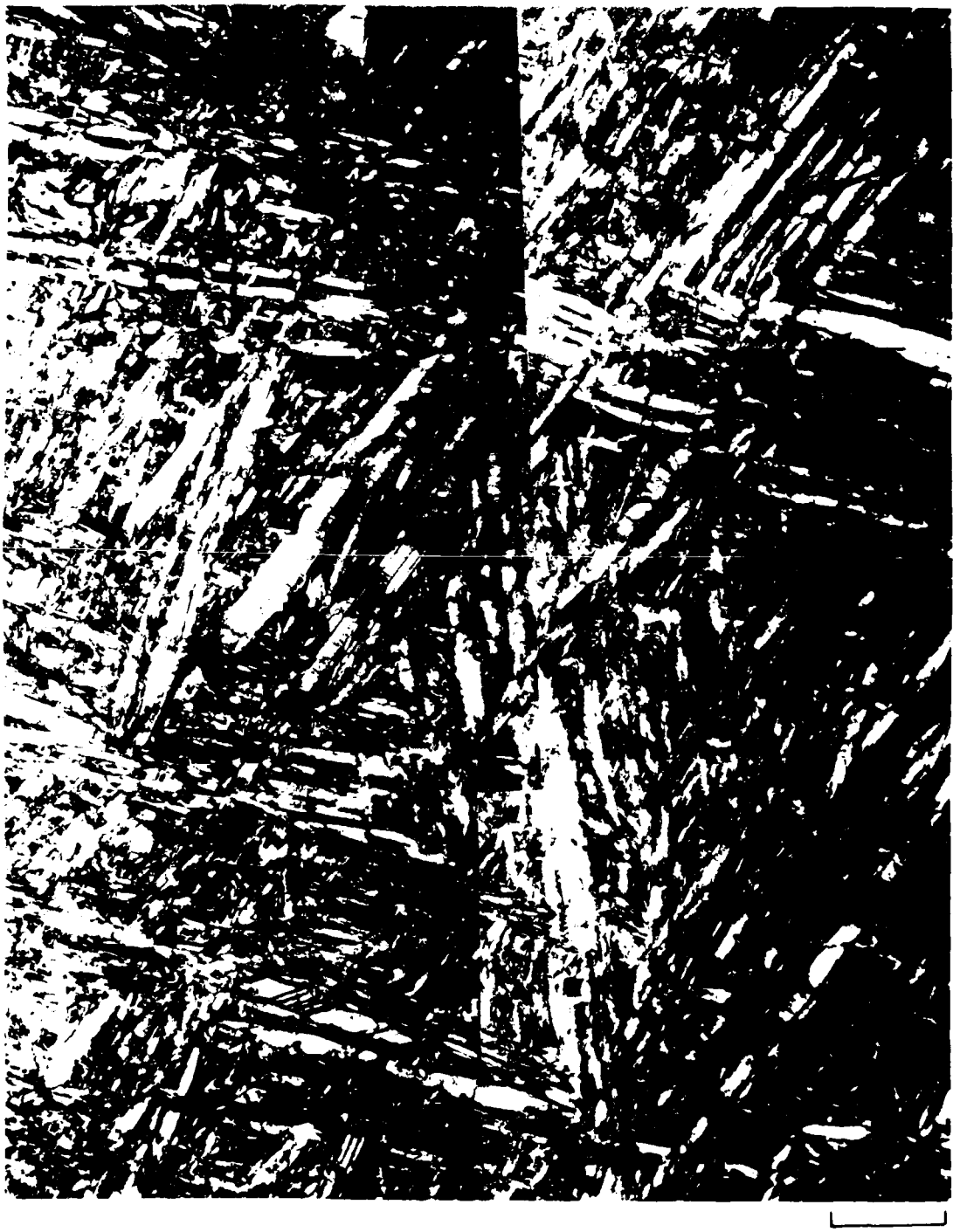

R82-915797-2

FIG. 28

α' HCP MARTENSITIC STRUCTURE OF FUSION ZONE LAYERGLAZE/NARROW GAP WELD SPECIMEN NO. 9

ENLARGED VIEW OF MICROSTRUCTURE IN FIG. 27

1 μm

NOTE THE GEOMETRIC PARTITIONING EFFECT IN WHICH THE α' LATHS ARE CONSTRAINED TO INCREASINGLY SHORTER LENGTHS AS THEY FORM SEQUENTIALLY. ONLY α IS PRESENT. STACKING FAULTS ARE VISIBLE AT (A) AND THE HIGH DISLOCATION DENSITY CHARACTERISTIC OF MANY α' LATHS IS IN CONTRAST AT (B).

82-8-94-24

STEM MICROGRAPH AND ASSOCIATED CHARACTERISTIC X-RAY SPECTRA

FUSION ZONE, LAYERGLAZE/NARROW GAP WELD SPECIMEN NUMBER 9

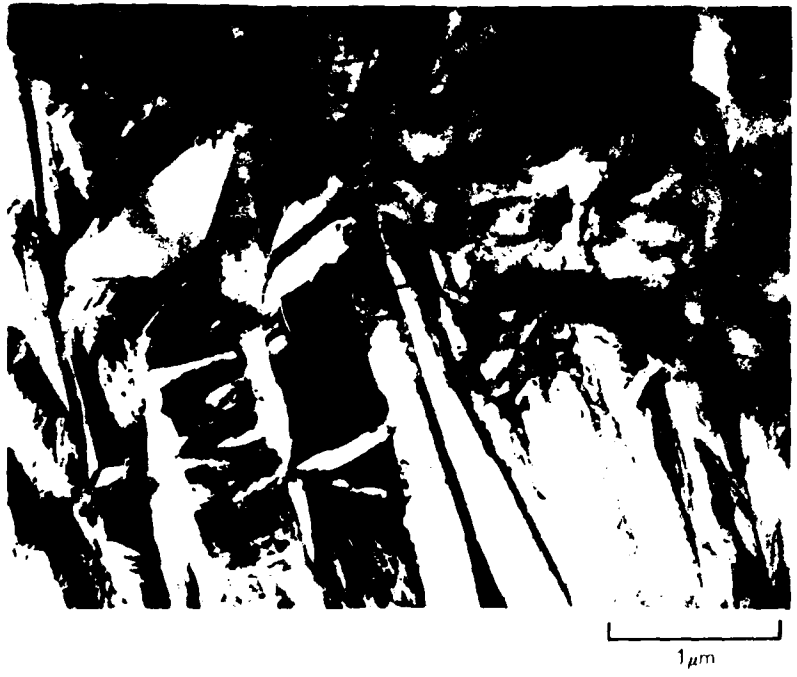

(a) STEM MICROGRAPH OF FUSION ZONE AREA FROM WHICH EDS DATA SHOWN IN (b) WERE OBTAINED. ARROWS MARK GRAIN BOUNDARY. "⊕" MARKS POSITION OF 50Å DIAMETER BEAM AT GRAIN BOUNDARY USED TO GENERATE DOT SPECTRUM SHOWN IN (b).

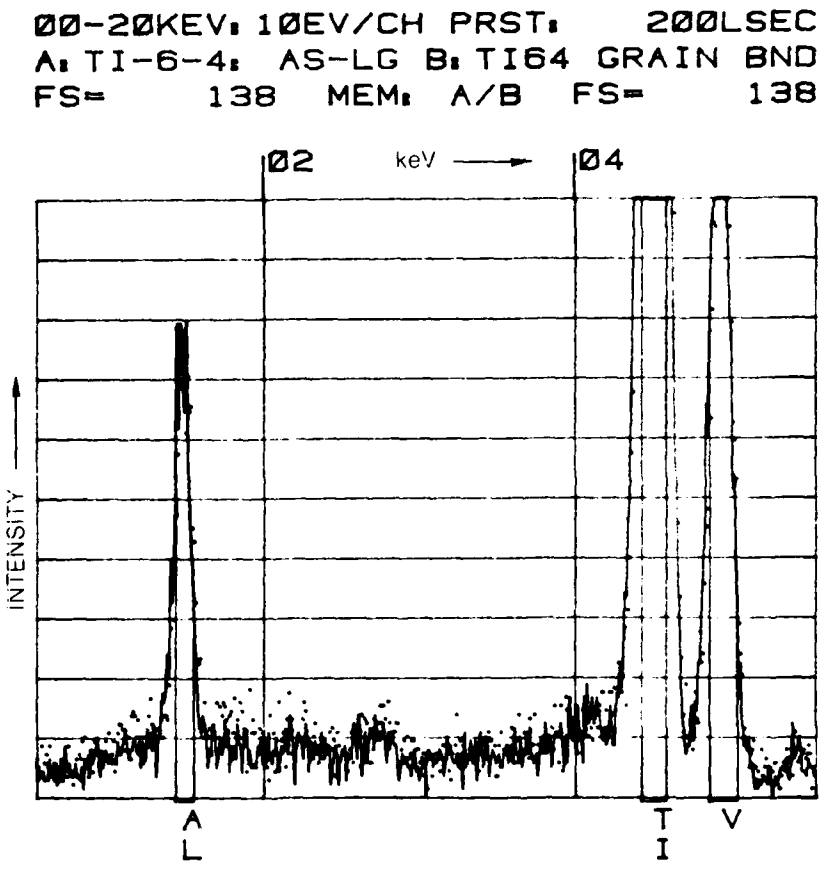

(b) EDS DATA FROM AREA SHOWN IN (a), ABOVE. NO APPARENT DIFFERENCE IN COMPOSITION BETWEEN SPECTRUM FROM ENTIRE AREA SHOWN IN (a) (LINE) AND SPECTRUM FROM A POINT ON THE GRAIN BOUNDARY (DOTS). ACCELERATING POTENTIAL 120kV. BEAM SPOT SIZE 50 Å

82-4-45-6

R82-915797-2

FIG. 29

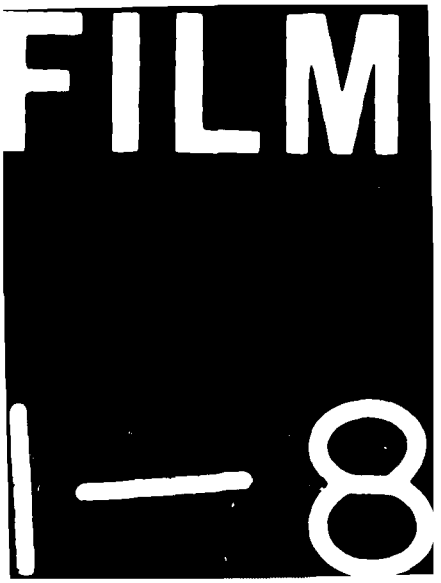
FILM
1-8